





# Multimomics analysis reveals the molecular mechanisms underlying virulence in *Rhizoctonia* and jasmonic acid-mediated resistance in Tartary buckwheat (*Fagopyrum tataricum*)

Yuqi He <sup>1,2,†</sup> Kaixuan Zhang <sup>1,†</sup> Shijuan Li <sup>1,3,†</sup> Xiang Lu <sup>1,4,†</sup> Hui Zhao <sup>1,†</sup>  
Chaonan Guan <sup>1,2,†</sup> Xu Huang <sup>1,†</sup> Yaliang Shi <sup>1</sup> Zhen Kang <sup>1</sup> Yu Fan <sup>1</sup> Wei Li <sup>1</sup>  
Cheng Chen <sup>1</sup> Guangsheng Li <sup>1</sup> Ou Long <sup>1</sup> Yuanyuan Chen <sup>1</sup> Mang Hu <sup>1</sup> Jianping Cheng <sup>4</sup>  
Bingliang Xu <sup>3</sup> Mark A. Chapman <sup>5</sup> Milen I. Georgiev <sup>6,7</sup> Alisdair R. Fernie <sup>7,8</sup>  
and Meiliang Zhou <sup>1,2,\*</sup>

- 1 Institute of Crop Sciences, Chinese Academy of Agricultural Sciences, National Crop Gene Bank Building, Beijing 100081, China
- 2 National Nanfan Research Institute, Chinese Academy of Agricultural Sciences, Sanya 572024, China
- 3 College of Plant Protection, Gansu Agricultural University, Lanzhou 730070, China
- 4 College of Agriculture, Guizhou University, Guiyang 550025, China
- 5 Biological Sciences, University of Southampton, Southampton SO17 1BJ, UK
- 6 Laboratory of Metabolomics, Institute of Microbiology, Bulgarian Academy of Sciences, Plovdiv 4000, Bulgaria
- 7 Center of Plant Systems Biology and Biotechnology, Plovdiv 4000, Bulgaria
- 8 Department of Molecular Physiology, Max-Planck-Institute of Molecular Plant Physiology, Potsdam 14476, Germany

\*Author for correspondence: [zhoumeiliang@caas.cn](mailto:zhoumeiliang@caas.cn)

†These authors contributed equally.

The author responsible for distribution of materials integral to the findings presented in this article in accordance with the policy described in the instructions for authors (<https://academic.oup.com/plcell/pages/General-Instructions>) is: Meiliang Zhou ([zhoumeiliang@caas.cn](mailto:zhoumeiliang@caas.cn)).

## Abstract

*Rhizoctonia solani* is a devastating soil-borne pathogen that seriously threatens the cultivation of economically important crops. Multiple strains with a very broad host range have been identified, but only 1 (AG1-IA, which causes rice sheath blight disease) has been examined in detail. Here, we analyzed AG4-HGI 3 originally isolated from Tartary buckwheat (*Fagopyrum tataricum*), but with a host range comparable to AG1-IA. Genome comparison reveals abundant pathogenicity genes in this strain. We used multimomic approaches to improve the efficiency of screening for disease resistance genes. Transcriptomes of the plant–fungi interaction identified differentially expressed genes associated with virulence in *Rhizoctonia* and resistance in Tartary buckwheat. Integration with jasmonate-mediated transcriptome and metabolome changes revealed a negative regulator of jasmonate signaling, cytochrome P450 (*FtCYP94C1*), as increasing disease resistance probably via accumulation of resistance-related flavonoids. The integration of resistance data for 320 Tartary buckwheat accessions identified a gene homolog to aspartic proteinase (*FtASP*), with peak expression following *R. solani* inoculation. *FtASP* exhibits no proteinase activity but functions as an antibacterial peptide that slows fungal growth. This work reveals a potential mechanism behind pathogen virulence and host resistance, which should accelerate the molecular breeding of resistant varieties in economically essential crops.

## Introduction

*Rhizoctonia solani*, belonging to the phylum Basidiomycota, is an aggressive soil-borne hemibiotrophic pathogen causing devastating diseases worldwide in a wide range of economically important crops, such as rice (*Oryza sativa*), wheat (*Triticum aestivum*), maize (*Zea mays*), potato (*Solanum tuberosum*), soybean (*Glycine max*), tomato (*Solanum lycopersicum*), sugar beet (*Beta vulgaris*), and cabbage (*Brassica oleracea*) (Yang and Li 2012). Plant defense against pathogen attack usually activates plant hormone signaling pathways involving jasmonic acid (JA), ethylene (ET), and salicylic acid (SA; Bari and Jones 2009; Kouzai et al. 2018). However, the precise mechanism of action of phytohormones in plant disease resistance is yet to be fully uncovered. At present, the control of *R. solani* in fields is highly dependent on chemical fungicides, while cultural practices and biological control have little effect (Molla et al. 2020). Given these facts, the development of genetically encoded resistance has become an ideal alternative approach to combat the pathogen.

Omics (genomics, transcriptomics, proteomics, and metabolomics) platforms have been used to understand pathogenesis and host defense in several studies. Draft genome sequences are available for different *R. solani* isolates representing 4 anastomosis groups (AGs), namely, rice AG1-IA (Zheng et al. 2013), lettuce (*Lactuca sativa*) AG1-IB (Wibberg et al. 2013, 2015), sugar beet AG2-2IIIB (Wibberg et al. 2016), potato AG3-PT (Wibberg et al. 2017), and wheat AG8 (Hane et al. 2014). Comparative genomic and transcriptomic studies of *R. solani* isolates have revealed differences in their genetic structure and gene expression profiles that may contribute to the host preference and virulence of this pathogen (Xia et al. 2017; Lee et al. 2021; Mat Razali et al. 2021). Metabolite profiles of *R. solani*-infected rice demonstrated an alteration of the glycolytic and oxidative pentose phosphate pathways as well as of secondary metabolism (Mutuku and Nose 2012). Quantitative trait locus (QTL) analysis for rice sheath blight resistance has been well studied and summarized (Molla et al. 2020; Li, Guo, et al. 2021; Li, Li, et al. 2021). Recently, genes associated with sheath blight resistance were identified in maize (Li et al. 2019) and rice (Wang, Shu, et al. 2021) by a genome-wide association study (GWAS).

Multinucleate *R. solani* isolates are divided into 14 physiologically and genetically distinct AGs (AG-1 to AG-13 and AGB1), some of which include several subgroups (Yang and Li 2012). *R. solani* AG4-HGI 3 was isolated from Tartary buckwheat (*Fagopyrum tataricum* [L.] Gaertn.) and can cause stem canker, damp-off, and death of seedlings, resulting in severe yield loss (Li, Zhang, et al. 2021). The genetic resistance of Tartary buckwheat against this disease, however, remains unknown. In this work, we report on the genome sequence of *R. solani* AG4-HGI 3 and performed a comparative analysis with the genomes of other *R. solani* isolates. We discovered a JA-induced response to *R. solani* in Tartary buckwheat when pathogen and host plants interact. Based on the

evaluation of the response to *R. solani* in 320 Tartary buckwheat accessions, we used GWAS to identify loci associated with disease resistance. We identified the 2 candidate resistance genes cytochrome P450 (*FtCYP94C1*) and aspartic proteinase (*FtASP*) and functionally analyzed them here. The genetic resource presented in this work should contribute to the development of effective techniques for controlling this devastating pathogen.

## Results

### Genome assembly identified abundant pathogenesis-related genes in *R. solani* AG4-HGI 3

To compare *R. solani* AG4-HGI 3 with other isolates, we explored candidate host crops of *R. solani* AG4-HGI 3. Inoculation experiments showed that the host range of *R. solani* AG4-HGI 3 is very extensive, as it infected not only the monocot plant species rice and wheat but also the species of Eudicots in the Brassicaceae, Cucurbitaceae, Leguminosae, Solanaceae, and Amaranthaceae families (cucumber [*Cucumis sativus*], lettuce, *Nicotiana benthamiana*, and tomato, among others; Supplemental Fig. S1). The broad host range of *R. solani* AG4-HGI 3 piqued our interest to study the mechanism underlying pathogenicity in this isolate. Staining with 4',6-diamidino-2-phenylindole (DAPI) demonstrated that *R. solani* AG4-HGI 3 is a multinucleate isolate, with the number of nuclei in a single cell varying (Supplemental Fig. S2). We determined the genome sequence of *R. solani* AG4-HGI 3 using Illumina HiSeq and PacBio sequencing platforms (Supplemental Data Set 1). The estimated genome size is 46.05 Mb with a heterozygous rate of ~1.49% (Supplemental Data Set 2), which was higher than that of most other multinucleus isolates, including *R. solani* AG1-IA (0.12%; Zheng et al. 2013) and AG1-XN (0.26%; Li, Guo, et al. 2021; Li, Li, et al. 2021). The assembled genome size is ~65.36 Mb, which is somewhat larger than the estimated genome size and that of most other *R. solani* isolates (Supplemental Data Sets 2 and 3 and Fig. S3). Accordingly, *R. solani* AG4-HGI 3 is predicted to contain at least 30% more protein-coding genes than all other sequenced *R. solani* isolates (Supplemental Fig. S4). However, the GC content (48.2%) was similar to that of other *R. solani* isolates. The scaffold N50 value is 568.8 kb, which is higher than that obtained from the assembled genomes of *R. solani* AG4 (Kaushik et al. 2022). We assessed the quality of the draft genome using the Benchmarking Universal Single-Copy Orthologs (BUSCO) and the Core Eukaryotic Gene Mapping Approach (CEGMA), with completeness scores of 94.1% and 95.97%, respectively, indicating the high quality of our genome assembly (Supplemental Data Set 4). Further, 30% of all genes appear to be duplicated according to the BUSCO analysis and randomly distributed on the scaffolds, which likely underlies the gene number expansion in this strain (Supplemental Fig. S5).

We identified a total of 438.6 kb (0.67%) of the *R. solani* AG4-HGI 3 genome as repeat containing, comprising 546



elements from 16 DNA transposons and retrotransposon families (Supplemental Data Set 5). These transposons are randomly distributed on the scaffolds (Supplemental Fig. S5). The content of repeat elements varies across isolates (Supplemental Data Set 6), and the proportion of repeat elements is lower in AG4-HGI 3 than in other *R. solani* isolates (Zheng et al. 2013; Hane et al. 2014; Lee et al. 2021). The transposon element long terminal repeat-vertebrate retrovirus 1 (LTR-ERV1) appeared the most abundant, accounting for 0.13% of total repetitive element length. The numbers of DNA, long interspersed nuclear element (LINE), satellite, and short interspersed nuclear element (SINE) transposons are modest compared to those from other isolates in *R. solani*, although some elements may have been missed in the more fragmented genomes of some isolates due to different sequencing and assembly strategies.

To investigate the phylogenetic relationships of all 23 *R. solani* available genomes in this work, we generated a maximum likelihood-based phylogenetic tree from single-copy orthogroups (Fig. 1A). We determined that *R. solani* AG4-HGI 3 is closely related to the other AG4 strains, AG4-HGI 1 and AG4-HGI 2. Moreover, a syntenic analysis also identified a large number of syntenic relationships between *R. solani* AG4-HGI 3 with other AG4 strains (Supplemental Fig. S6), confirming the close relationship between these strains. Genome comparison demonstrated that *R. solani* contains 9,630 orthogroups absent from *Magnaporthe oryzae* (Supplemental Data Set 7). Among them, 664 orthogroups were specific to *R. solani* AG4, of which 131 orthogroups are shared by the 3 isolates, and 350 orthogroups are specific to *R. solani* AG4-HGI 3 (Supplemental Data Set 8). We also identified 3,236 significantly expanded gene families (consisting of 11,339 genes) and 891 significantly contracted gene families (comprising 103 genes) ( $P < 0.05$  computed with CAFÉ) in *R. solani* AG4-HGI 3 (Figs. 1A and S7 and Supplemental Data Set 9). Of the 891 contracted gene families, 801 were apparently entirely absent in strain AG4-HGI 3. A gene ontology (GO) term enrichment analysis revealed that the expanded gene families are mainly enriched in catalytic activity and ion binding (Fig. 1B). Of the genes in the expanded gene families, 394 were involved in glycosyl hydrolysis activity, and 74 were involved in pectate lyase activity. As the plant cell wall is mainly composed of cellulose, hemicellulose, and pectin and cell wall degradation is closely associated with the saprophytic lifestyle of fungi (Cantarel et al. 2009), the expansion of these cell wall degradation-related genes might be responsible for the broad host range of *R. solani* AG4-HGI 3.

Considering the broad host range of *R. solani* AG4-HGI 3, and given that the pathogenicity genes encoding carbohydrate-active enzymes (CAZymes), secreted proteins, and effectors are prime weapons for pathogen infection and modulation of host morphology (Zheng et al. 2013; Kaushik et al. 2022), we turned our attention to these pathogenicity genes. CAZymes are necessary for phytopathogenic organisms to degrade the structural components of the cell wall

and hence enter their host plants (Cantarel et al. 2009). We therefore characterized the CAZyme complement in *R. solani* and *M. oryzae*. We predicted a total of 1,026 CAZymes in *R. solani* AG4-HGI 3 (Supplemental Data Set 10 and Fig. S5), accounting for 5.45% of all protein-coding genes, which was greater than in some isolates of *R. solani* (AG1-IA, AG1-IB-7/3/14, AG3-PT-1AP, and AG8-WAC10335) and *M. oryzae* (Supplemental Data Set 11, Supplemental Figure S8). We identified a greater proportion of CAZymes involved in lignin, cellulose, hemicellulose, and pectin degradation in *R. solani* AG4-HGI 3 compared to AG1-IA and AG8-WAC10335 (Fig. 1A and Supplemental Data Set 12), which was in accordance with the expanded number of genes related to glycosyl hydrolysis and pectate lyase activity in *R. solani* AG4-HGI 3. Secreted proteins are essential in inhibiting the defense response of host cells (Lee et al. 2021): we predicted a total of 1,167 secreted proteins in *R. solani* AG4-HGI 3 (Supplemental Data Set 13), accounting for 6.20% of all protein-coding genes, which is relatively lower than in most other *R. solani* isolates (Supplemental Data Set 14). Moreover, we identified relatively fewer predicted effectors in AG4-HGI 3 (accounting for 1.56% of the protein-coding genes) relative to most other strains (Supplemental Data Sets 15 and 16). In addition, the proportion of CAZymes was higher in most *R. solani* strains compared to *M. oryzae*, while *R. solani* was characterized by a smaller proportion of secreted proteins and effectors than *M. oryzae*. These findings might be an important feature that distinguishes this species from *M. oryzae*, and in accordance with previous work demonstrating fewer secreted proteins in *R. solani* than in other filamentous pathogens (Anderson et al. 2017). Moreover, we predicted 2,355 virulence genes, 3,099 pathogen–host interaction genes, 2,124 transporter genes, 2,071 transmembrane protein genes, and 19 secondary metabolite biosynthesis gene clusters in *R. solani* AG4-HGI 3 (Supplemental Data Sets 17 to 21). These candidate genes are randomly distributed across the scaffolds (Supplemental Fig. S5) and represent a valuable resource to reveal the intimate mechanism of *R. solani* infection of susceptible plant species.

### Upregulated pathogenesis-related genes are involved in *R. solani* AG4-HGI 3 infection of Tartary buckwheat

To gain insight into the pathogenesis of *R. solani* AG4-HGI 3 infection of Tartary buckwheat, we performed an RNA-seq analysis of *R. solani* AG4-HGI 3 at 3 infection stages (6 h, water-soaked spots appeared; 14 h, spots expansion significantly; and 22 h, rotten and necrotic spots appeared) using the assembled genome of *R. solani* AG4-HGI 3 as a reference (Supplemental Fig. S9 and Data Set 22). The strain without host infection was used as negative control. In total, we determined that 19,140 genes (including 18,821 protein-coding genes, 265 transfer RNAs [tRNAs], and 54 ribosomal RNAs [rRNAs]) are expressed at some point during infection. Of these, 16.8% (3,215 out of 19,140) were upregulated in at

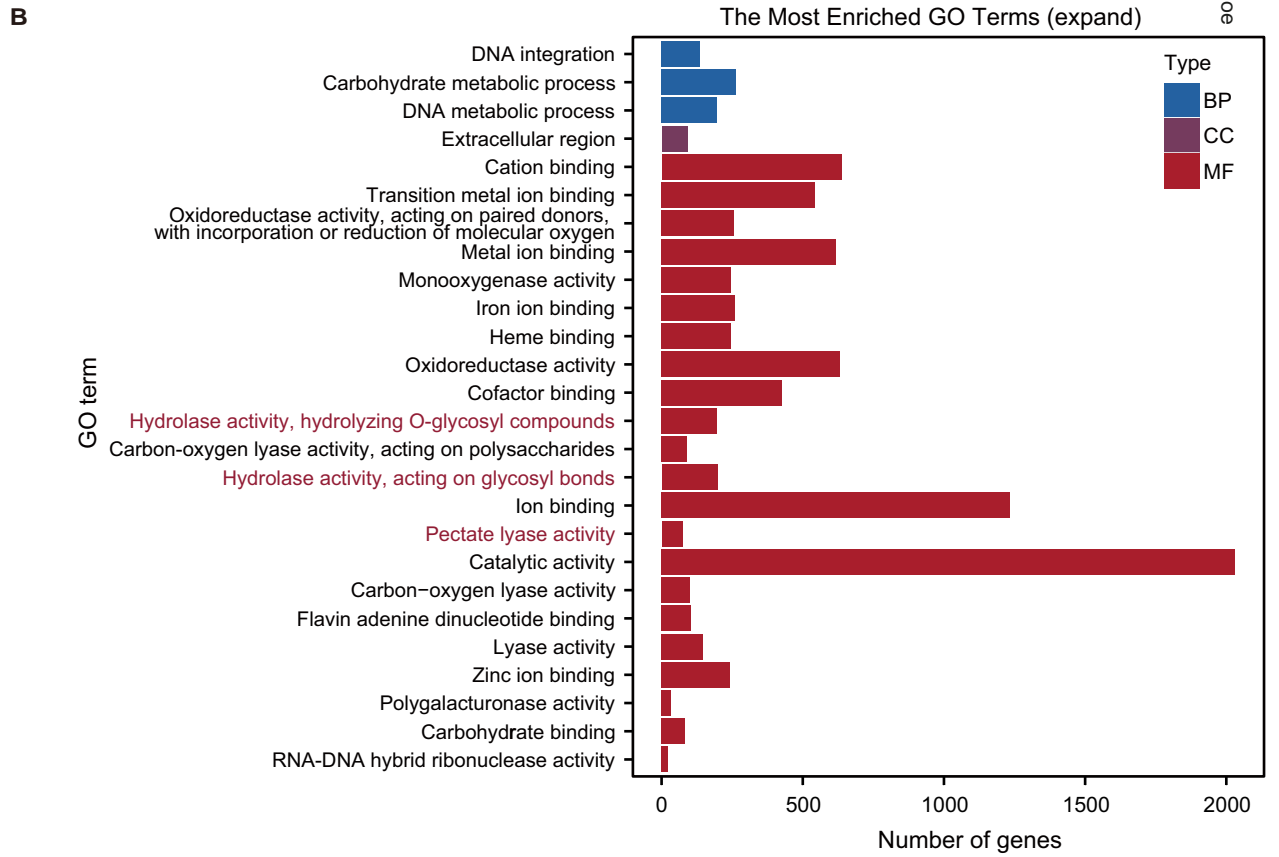
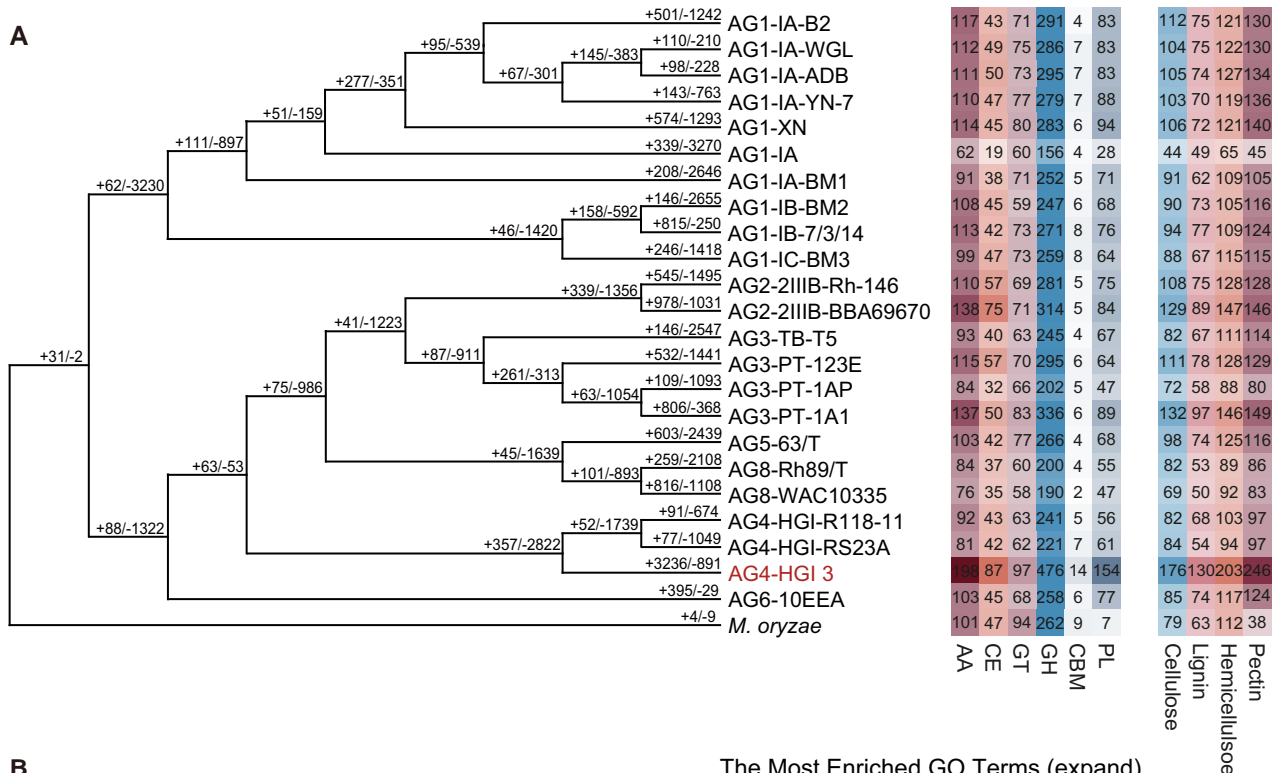


**Figure 1.** Expansion of cell wall degradation enzymes in *R. solani* AG4-HGI 3. **A)** Phylogenetic tree depicting the relationships among the genomes of 23 *R. solani* strains (left). The phylogenetic tree was reconstructed using the maximum likelihood approach based on single-copy orthogroups and rooted with *M. oryzae*. Numbers on each branch indicate the number of expanded (positive numbers) and contracted (negative number) gene families. The numbers of CAZyme genes in 23 *R. solani* isolates and *M. oryzae* are shown (right). Different colors represent different types of

(continued)

least 1 time point and 270 genes were upregulated at all time points (Supplemental Data Set 23 and Fig. S10). Further, 503 genes were upregulated within the first 6 h of Tartary buckwheat infection by *R. solani* AG4-HGI 3 (Fig. 2A), rising dramatically after infection for 14 h to 2,102 genes, while slightly increasing after 22 h of infection (2,655 genes), suggesting that the transcriptome of *R. solani* AG4-HGI 3 reacts strongly after 14 h of infection. We analyzed the functions of all 3,215 upregulated genes according to their annotation in the assembled genome. In total, 477 virulence genes, 401 genes encoding secreted proteins, 695 genes encoding pathogen-host interaction proteins, and 107 genes encoding effectors were upregulated in at least 1 time point (Fig. 2B and Supplemental Data Set 23). A Kyoto Encyclopedia of Genes and Genomes (KEGG) pathway enrichment analysis revealed that the highly expressed transcripts are significantly enriched in the ribosome (Fig. 2C), suggesting that transcript translation is metabolically active during *R. solani* AG4-HGI 3 infection of Tartary buckwheat. The list of these upregulated pathogenesis-related genes will undoubtedly provide further clues to reveal the mechanism during *R. solani* AG4-HGI 3 infection of Tartary buckwheat.

We also analyzed the expression level of expanded gene families in *R. solani* AG4-HGI during infection of Tartary buckwheat (Supplemental Data Sets 24 to 27). Most (>70%) of the genes in expanded gene families exhibited no significant change during infection of Tartary buckwheat. Less than a quarter of expanded gene families exhibited more differentially expressed genes than unchanged genes. In addition, the proportions of upregulated and downregulated genes in expanded gene families were lower than that for the whole genome following infection for 6 and 22 h, while we observed the opposite pattern 14 h into infection, further confirming that this time point is crucial for *R. solani* AG4-HGI 3 infection. Less than a quarter of expanded gene families exhibited larger proportions of upregulated or downregulated genes than that for the whole genome. We conducted GO and KEGG analyses to investigate the expression pattern of expanded gene families with specific functions (Supplemental Figs. S11 and S12). We observed that the upregulated expanded gene families are mainly enriched in genes related to pentose and glucuronate interconversion, cyanoamino acid metabolism, ribosome, starch and sucrose metabolism, and cysteine and methionine metabolism. The downregulated expanded gene families were mainly enriched in genes related to glycolysis/gluconeogenesis, amino sugar and nucleotide sugar metabolism, methane metabolism, arginine and proline metabolism, and ABC transporters.

As with expanded gene families, the expression level of most genes in contracted gene families exhibited no changes during infection of Tartary buckwheat (Supplemental Data Sets 28 to 31). Less than 3% of contracted gene families had more differentially expressed genes than unchanged genes. In addition, the proportions of upregulated and downregulated genes in contracted gene families were higher than that for the whole genome. Less than 2.5% of contracted gene families exhibited larger proportion of upregulated or downregulated genes than that for the whole genome. GO and KEGG analyses revealed that the upregulated contracted gene families are mainly enriched in genes related to sulfur metabolism, carbon metabolism, lysine degradation, monobactam biosynthesis, and riboflavin metabolism (Supplemental Figs. S13 and S14). The downregulated contracted gene families were mainly enriched in genes related to glycolysis/gluconeogenesis, pyruvate metabolism, glycerophospholipid metabolism, and carbon metabolism. The varied gene number and expression level of these gene families with specific functions may help further reveal the infection mechanism of *R. solani* AG4-HGI 3.

As comparative genomics revealed that *R. solani* AG4-HGI 3 has more CAZyme genes than other *R. solani* isolates, we examined the expression levels of genes encoding CAZymes during *R. solani* AG4-HGI 3 infection of Tartary buckwheat in detail. Overall, nearly half (467 out of 1,026) of all genes encoding CAZymes were upregulated in at least 1 time point during Tartary buckwheat infection by *R. solani* (Supplemental Data Sets 32 and 33). Notably, 424 CAZyme genes were upregulated at 14 h into infection, which was more than at 6 (76 genes) and 22 h (387 genes), suggesting that this period is important for the degradation of the cell wall of Tartary buckwheat by *R. solani*. Further analysis indicated that 106 of these upregulated CAZymes were involved in cellulose degradation and another 117 were involved in hemicellulose degradation, 174 in pectin degradation, and 35 in lignin degradation (Fig. 2D and Supplemental Data Set 34). Identification of these upregulated CAZyme genes will help reveal specific components of the plant cell wall degradation machinery during *R. solani* infection.

To investigate the mechanism of *R. solani* AG4-HGI 3 infection of Tartary buckwheat, we assessed the functions of virulence genes experimentally by transient heterologous expression in *N. benthamiana* leaves. We chose YTH domain-containing protein (*RsYTHDC*, gene04142), proline-rich protein (*RsPRP*, gene00437), and laminin domain-containing protein (*RsLDLP*, gene15409), which are homologs of virulence genes (AG1IA\_00579, AG1IA\_04049, and AG1IA\_06427) previously identified in *R. solani* AG1-IA (Zheng et al. 2013). *D-Arabinitol 2-dehydrogenase* (*RsDAD*, gene08192) is a *R. solani* AG4-HGI

(Figure 1. Continued)

CAZyme genes, with the intensity of colors being proportional to the number of genes. AA, auxiliary activity; CE, carbohydrate esterase; GT, glycosyl transferase; GH, glycoside hydrolase; CBM, carbohydrate-binding module; PL, polysaccharide lyase. **B)** Most significantly enriched GO terms of expanded gene families in *R. solani* AG4-HGI 3. Enriched pathways related to glycosyl hydrolysis and pectate lyase are shown in red. BP, biological process; MF, molecular function; CC, cellular component.



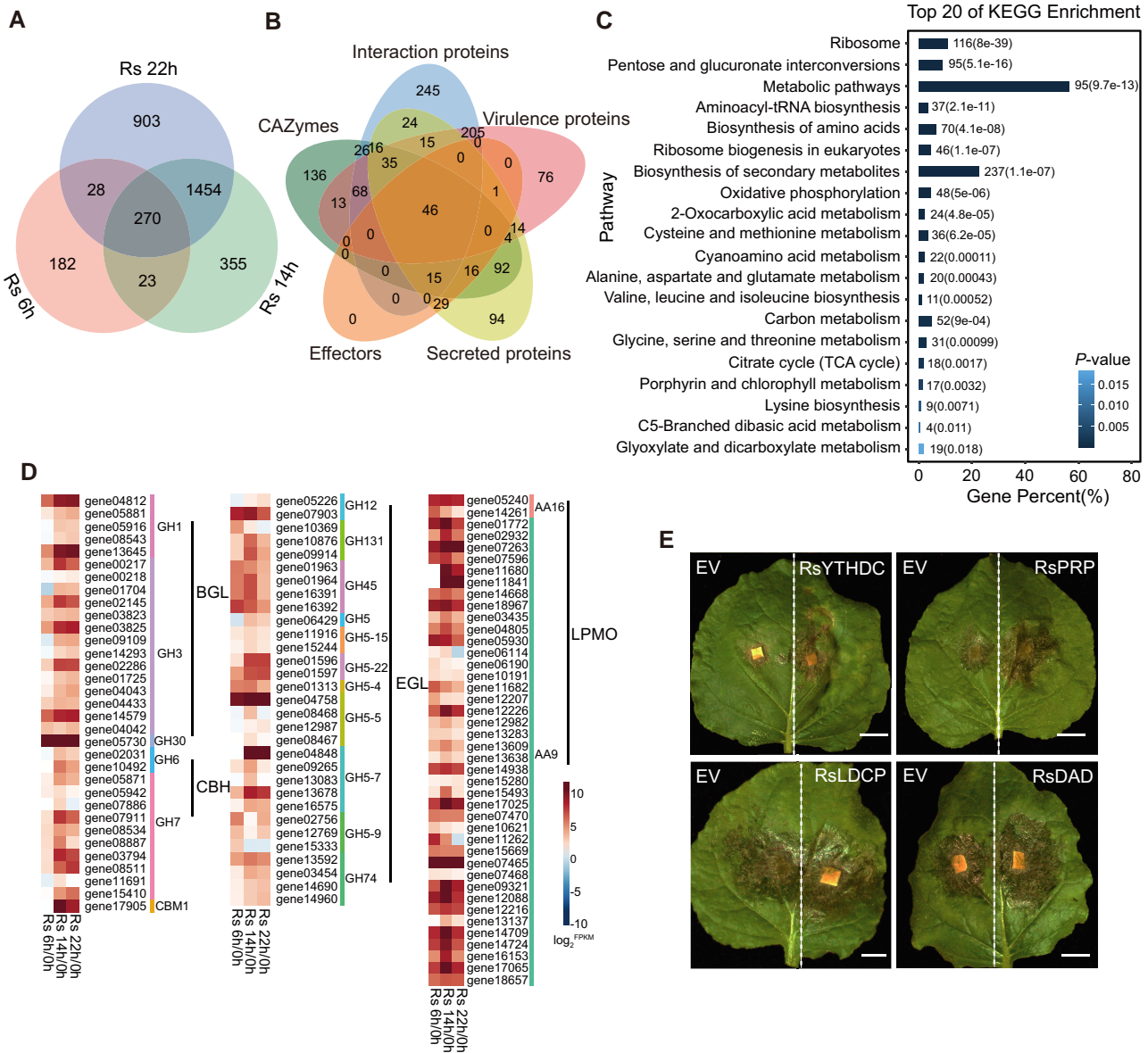


**Figure 2.** Differentially expressed *R. solani* genes during infection of Tartary buckwheat. **A)** Venn diagram showing the number of commonly and uniquely upregulated genes from *R. solani* AG4-HGI 3 during the *R. solani*–Tartary buckwheat interaction for 6 (RS 6 h), 14 (RS 14 h), and 22 h (RS 22 h). Mycelial disks subcultured on PDA medium were used to infect the leaves of 21-d-old Tartary buckwheat seedlings for the indicated times before the leaves were harvested for transcriptome analysis. Three independent biological replicates ( $n = 10$  seedlings each) for each treatment were conducted. Genes with adjusted  $P \leq 0.05$  and fold change  $> 2$  (compared to noninoculated control samples) were considered to be significantly differentially expressed genes and used for analysis. RS, *R. solani*. **B)** Venn diagram showing the overlap between upregulated genes encoding predicted CAZymes, effectors, secreted proteins, virulence proteins, and interaction proteins in *R. solani* AG4-HGI 3 during infection of Tartary buckwheat. **C)** Most significantly enriched KEGG metabolic pathways of upregulated genes from *R. solani* AG4-HGI 3 during the infection of Tartary buckwheat by *R. solani*. Numbers next to the bars indicate the  $P$ -values. **D)** Heatmap showing the gene expression pattern of *R. solani* AG4-HGI 3–upregulated CAZyme genes involved in cellulose degradation during *R. solani* infection of Tartary buckwheat for 6 (Rs 6 h/0 h), 14 (Rs 14 h/0 h), and 22 h (Rs 22 h/0 h). Intensity of the colors is proportional to  $\log_2FC$ . GH, glycoside hydrolase; CBM, carbohydrate-binding module; AA, auxiliary activity; BGL,  $\beta$ -glucosidase; CBH, cellobiohydrolase; EGL, endoglucanase; LPMO, lytic polysaccharide monoxygenase. **E)** Phenotypes observed on *N. benthamiana* leaves heterologously expressing RsYTHDC, RsLDPC, RsPRP, or RsDAD and infected with *R. solani* AG4-HGI 3. *N. benthamiana* leaves were inoculated with subcultured mycelial disks for 2 d. Leaves transiently infiltrated with the empty vector (EV) control and then infected by *R. solani* AG4-HGI 3 were used as negative control. The phenotypes were observed in leaves of 3 independently infiltrated *N. benthamiana* seedlings ( $n = 3$ ). The experiments were performed 3 times using different batches of *N. benthamiana* seedlings with similar results. Photographs of *N. benthamiana* leaves from 1 representative experiment are shown. Scale bars, 1 cm.

3-specific interacting virulence gene that is significantly upregulated during *R. solani* AG4-HGI 3 infection for 14 and 22 h. We individually expressed *RsYTHDC*, *RsPRP*, *RsLDCP*, and *RsDAD* from *R. solani* AG4-HGI 3 in *N. benthamiana* leaves (Supplemental Fig. S15) and evaluated disease resistance following subculture with mycelial disks for 48 h. None these 4 virulence genes caused any morphological changes to the infiltrated leaves in normal growth conditions (Supplemental Fig. S16) but significantly enhanced disease susceptibility compared to the control, as measured by relative fungal biomass and MDA content (Figs. 2E, S17, and S18), suggesting that these virulence genes might help pathogens infect host plants successfully.

To explore the function of these virulence proteins in plants, we determined the subcellular localization of *RsYTHDC* and *RsDAD* fused to the green fluorescent protein (GFP). A transient *N. benthamiana* expression assay indicated that *RsYTHDC* and *RsDAD* localize in both the cytoplasm and nucleus (Supplemental Fig. S19), suggesting that these virulence factors may help pathogen infection by interacting with plant proteins. We also looked for proteins interacting with *RsYTHDC* or *RsDAD* using a combination of pull-down and mass spectrometry method (Supplemental Fig. S20; Brymora et al. 2004). We obtained 236 and 192 candidate proteins that might interact with *RsYTHDC* or *RsDAD*, respectively (Supplemental Data Sets 35 and 36). Most homologs of the candidate *RsYTHDC*-interacting proteins were previously described to confer disease resistance, including endochitinase (FtPinG0404899000) (Bai et al. 2021), aquaporin (FtPinG0606269900) (Tian et al. 2016), polygalacturonase-inhibiting protein (FtPinG0505912500 and FtPinG0707633000) (Borras-Hidalgo et al. 2012), UDP-glycosyltransferase (FtPinG0707681200) (Pasquet et al. 2016; He et al. 2020), mitogen-activated protein kinase (FtPinG0505354900) (Wang, Shao, et al. 2021), oxalate-CoA ligase (FtPinG0201520900) (Peng et al. 2017), cationic peroxidase (FtPinG0606353800) (Wally and Punja 2010), annexin (FtPinG0404585800) (Zhao et al. 2019), vacuolar-processing enzyme like (FtPinG0303401000) (Wang et al. 2017; Dong et al. 2022), and protein THYLAKOID FORMATION1 (FtPinG0808541100) (Wangdi et al. 2010). Likewise, homologs of some candidate *RsDAD*-interacting proteins have been previously shown to enhance disease resistance: major latex protein (FtPinG0100209300) (Yang et al. 2015), chorismate synthase (FtPinG0505432600) (Hu et al. 2009), peptide methionine sulfoxide reductase (FtPinG0100988800) (Oh et al. 2010), serine hydroxymethyltransferase (FtPinG0202435800) (Moreno et al. 2005), and L-ascorbate peroxidase (FtPinG0403764100) (Liu et al. 2018). Homologs of other putative interactors with *RsDAD* included disease susceptibility genes encoding nucleoside diphosphate kinase (FtPinG0707189500 and FtPinG0808916000) (Ye et al. 2020), isocitrate dehydrogenase (FtPinG0505344500) (Mhamdi et al. 2010), monodehydroascorbate reductase (FtPinG0404369900) (Feng et al. 2014), ferredoxin-dependent glutamate synthase (FtPinG0707851300) (Chen et al. 2016),

and phosphate transporter (FtPinG0707291400) (Dong et al. 2019). We employed bimolecular fluorescence complementation (BiFC) assays to verify the interaction between the virulence proteins and their candidate interacting proteins. We established that a serine hydroxymethyltransferase (FtSHMT, FtPinG0202435800) can interact with the virulence protein *RsDAD*, suggesting the reliability of these candidate interacting proteins (Supplemental Fig. S21). However, as the function of their encoding genes in Tartary buckwheat response to *R. solani* AG4-HGI 3 infection might be varied, further study is needed to ascertain the function of these candidate interacting proteins.

### JA is involved in Tartary buckwheat resistance to *R. solani* AG4-HGI 3

Although the study of the fungal genome and the plant–fungus interaction transcriptome can help us understand the pathogenesis of the strains, how plants respond to these fungal infections remains unclear. Through studying the mechanism of host plant response to pathogens, exploitation and utilization of disease resistance genes represent an important means to improve the disease resistance of host plants. To better understand the host plant response to *R. solani*, we analyzed the transcriptomes of Tartary buckwheat in response to *R. solani* AG4-HGI 3 infection (Supplemental Data Set 37). In total, 48.5% (17,745 out of 36,613) of Tartary buckwheat genes were differentially expressed in at least 1 time point during *R. solani* AG4-HGI 3 infection (Supplemental Data Set 38 and Fig. S22). Again, the number of differentially expressed genes peaked at 14 (14,698 genes) and 22 h (15,200 genes), nearly twice as many as at 6 h (7,773 genes), suggesting that the Tartary buckwheat transcriptomic response to infection is greatest when the pathogen is most active. A KEGG analysis revealed that a large fraction of differentially expressed genes is involved in plant secondary metabolite biosynthesis, as well as phytohormone signaling (Fig. 3A), suggesting that these pathways are of critical importance to the plant response to *R. solani* infection.

We investigated the function of disease-related phytohormones on plant defense against *R. solani*, by evaluating disease resistance of Tartary buckwheat seedlings pretreated with the phytohormones gibberellin (GA), ET, SA, and JA (Supplemental Fig. S23). We observed that the sunken lesion and dark brown symptoms are visibly alleviated in Tartary buckwheat seedlings pretreated with JA, but not with other phytohormones, compared to the control pretreated with DMSO. We thus speculated that JA might play an important role in Tartary buckwheat defense against *R. solani* AG4-HGI 3 infection. As JA is a plant hormone that plays important roles in the regulation of plant secondary metabolites biosynthesis and disease resistance (Bari and Jones 2009; De Geyter et al. 2012; Verma et al. 2016; Zhou and Memelink 2016), we focused on the expression level of genes involved in JA biosynthesis and signaling. In total, 62 differentially expressed genes appeared involved in JA biosynthesis and signaling (Fig. 3B and Supplemental Data Set 39), suggesting that JA

signal transduction plays an important role during *R. solani* infection of Tartary buckwheat.

As numerous JA signaling genes were differentially expressed during *R. solani* infection, we studied the involvement of JA signaling during host plant response to *R. solani* infection. To this end, we determined the kinetic response of the transcriptome following methyl jasmonate (MeJA) treatment at different time intervals (1, 4, and 12 h; i.e. the early stages of infection where the greatest responses are seen by both the pathogen and the plant; [Supplemental Data Set 40](#)). We identified the Tartary buckwheat genes that are differentially expressed during *R. solani* infection and following MeJA treatment. We established that 29.3% (5,205 out of 17,745) of the genes differentially expressed during *R. solani* infection are also differentially expressed following MeJA treatment ([Fig. 3C](#); [Supplemental Data Set 41](#) and [Fig. S24](#)), confirming that JA signaling plays an essential role in Tartary buckwheat response to *R. solani*. A KEGG analysis revealed that many differentially expressed genes are involved in phenylpropanoid and flavonoid biosynthesis ([Fig. 3D](#)). As previous research has shown that JA can regulate flavonoid biosynthesis ([Zhou et al. 2017](#); [Zhang, Yohe, et al. 2018](#), [Zhang, Logacheva, et al. 2018](#); [Chen et al. 2019](#); [Ding et al. 2021](#)) and flavonoids are involved in biotic stress responses ([Misra et al. 2010](#); [Ullah et al. 2017](#)), we speculated that JA might regulate flavonoids biosynthesis, hence modulating the disease resistance of Tartary buckwheat.

Of the above genes significantly upregulated during *R. solani* infection and MeJA treatment, we characterized the JA signaling transduction gene *FtCYP94C1* (FtPinG0808388800), homologous to *Arabidopsis CYP94C1*, encoding an enzyme responsible for JA-Ile oxidation to 12OH-JA-Ile ([Heitz et al. 2012](#)) ([Fig. 4, A to C](#)). Heterologous expression of *FtCYP94C1* in *Arabidopsis* or its overexpression in Tartary buckwheat exhibited no change in phenotype compared to wild-type plants, while resulting in significantly enhanced disease resistance compared to the controls ([Figs. 4, D and E](#), and [S25 to S28](#)), as also described in its homolog gene in *Arabidopsis* ([Poudel et al. 2019](#)). Various JA biosynthesis and signaling mutants (*aoc4*, *jar1* [*jasmonate resistant 1*], and *myc2 myc3 myc4*) displayed decreased disease resistance compared to the controls ([Supplemental Figs. S29 to S31](#)), and pretreatment with JA increased their disease resistance index, suggesting a positive role for JA signaling on plant defense against *R. solani* AG4-HGI 3. However, the disease resistance ability of *FtCYP94C1* was in contrast with the well-known reduced capacity of 12OH-JA-Ile in promoting the formation of the CORONATINE INSENSITIVE 1–JASMONATE-ZIM-DOMAIN PROTEIN 1 (COI1–JAZ) receptor complex ([Koo et al. 2011](#); [Heitz et al. 2012](#); [Koo et al. 2014](#)) and the positive regulation disease resistance by JA signaling ([Verma et al. 2016](#); [Pan et al. 2020](#)), suggesting that *FtCYP94C1* may regulate Tartary buckwheat resistance to *R. solani* through other pathways beside typical JA signaling. As many genes differentially expressed during both *R. solani* infection and MeJA treatment were involved in flavonoid biosynthesis and the positive

regulation of 12OH-JA-Ile in flavonoid biosynthesis ([Poudel et al. 2019](#)), we analyzed the metabolome of *FtCYP94C1* overexpression *Arabidopsis* lines to investigate the metabolic changes involved in disease resistance ([Supplemental Fig. S32 and Data Set 42](#)). 12OH-JA-Ile significantly accumulated in *FtCYP94C1* overexpression lines, confirming that *FtCYP94C1* is responsible for JA-Ile oxidation to 12OH-JA-Ile. Moreover, the flavonoids including rutin, quercitrin, and chalcone also accumulated in *FtCYP94C1* overexpression lines ([Fig. 4F](#)). Flavonoid contents significantly decreased in JA biosynthesis and signaling mutants (*aoc4*, *jar1*, and *myc2 myc3 myc4*; [Supplemental Fig. S33](#)) and significantly increased after JA treatment, suggesting a positive role for typical JA signaling on flavonoid content. As flavonoids have been previously reported to enhance disease resistance ([Yamamoto et al. 2000](#); [Misra et al. 2010](#); [Yang et al. 2016](#); [Schenke et al. 2019](#)), we speculate that *FtCYP94C1* may not function through the typical JA signaling pathway by promoting the formation of COI1–JAZ receptor complex but rather by increasing the accumulation of disease resistance–related flavonoids.

We noticed that the expression of genes encoding some of the candidate proteins interacting with the virulence proteins RsYTHDC and RsDAD respond to both *R. solani* infection and MeJA treatment. Among them, homolog of UDP-glycosyltransferase (FtPinG0707681200) is involved in the biosynthesis of plant disease–related secondary metabolites ([Pasquet et al. 2016](#); [He et al. 2020](#)). Homologs of polygalacturonase-inhibiting proteins (FtPinG0505912500 and FtPinG0707633000) are structural glycoproteins of the plant cell wall with antifungal activity; they can specifically bind to and inhibit fungal polygalacturonases ([Ferrari et al. 2003](#)). The expression of these disease resistance genes was mostly upregulated after both *R. solani* infection and MeJA treatment ([Supplemental Data Sets 35 and 36](#)), as previously reported in *Arabidopsis* and golden root (*Rhodiola sachalinensis*) ([Ferrari et al. 2003](#); [Yu et al. 2011](#)). The possible interaction between virulence proteins and these disease resistance proteins may result in the dysfunction of resistance proteins, hence reducing the plant immune response and helping pathogens infect their host successfully. We speculate that the JA–induced expression of these disease resistance genes may alleviate the dysfunction of their encoded resistance proteins, thus helping Tartary buckwheat better resist pathogen infection. However, this conjecture needs to be tested.

### Integrating GWAS and gene expression data to accurately identify candidate genes that confer resistance to *R. solani* AG4-HGI 3 in Tartary buckwheat

Although the JA signaling pathway gene *FtCYP94C1* was demonstrated above to be connected to Tartary buckwheat resistant to *R. solani* AG4-HGI 3, the functions of many other Tartary buckwheat genes differentially expressed during



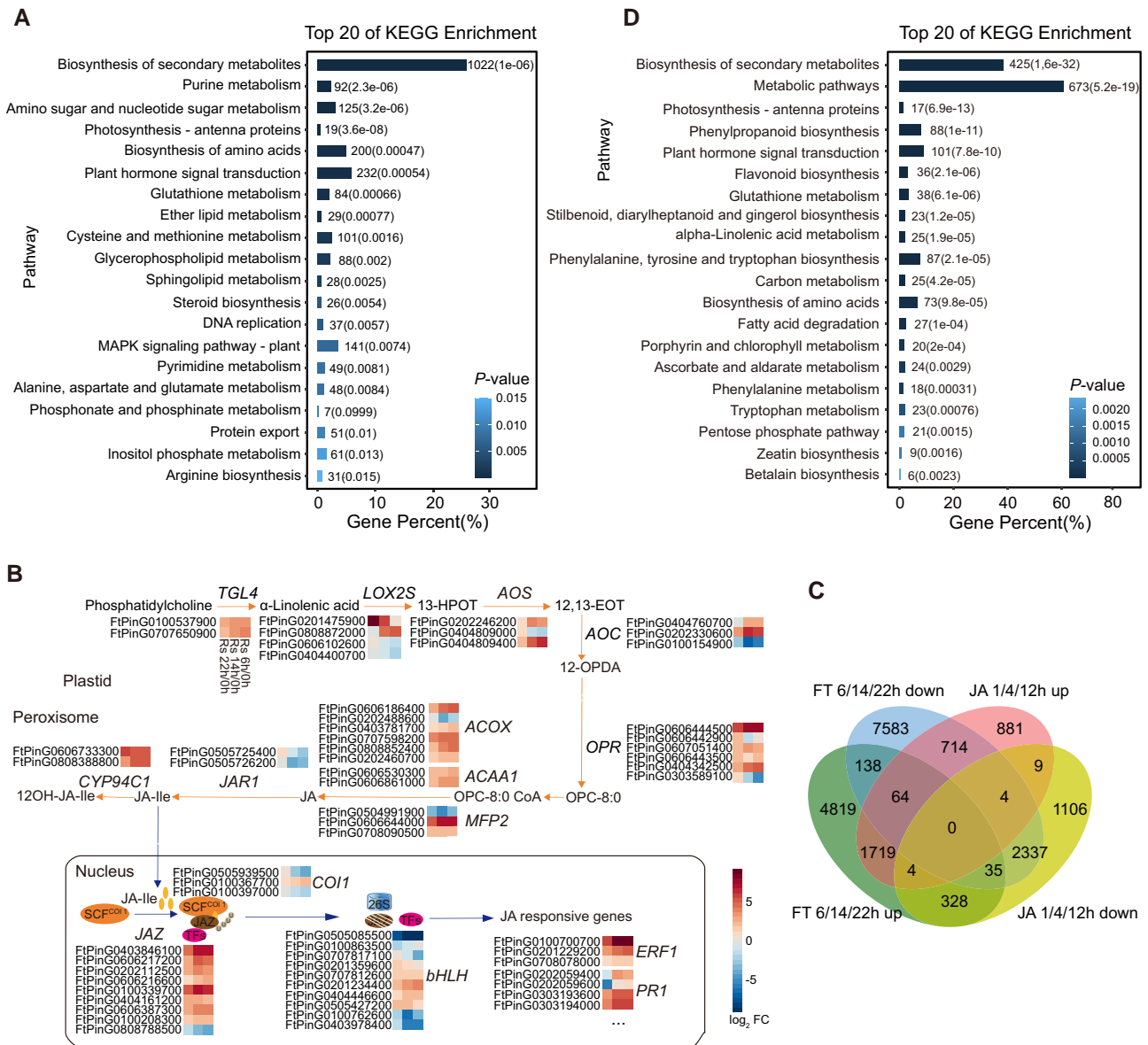


**Figure 3.** Differentially expressed genes from Tartary buckwheat during *R. solani* infection. **A**) Most significantly enriched KEGG metabolic pathways among differentially expressed genes of Tartary buckwheat during *R. solani* infection. The leaves of 21-d-old Tartary buckwheat seedlings were inoculated with mycelial disks subcultured on PDA medium for 6, 14, or 22 h before being collected for transcriptome analysis. Three independent biological replicates ( $n = 10$  seedlings each) for each treatment were conducted. Genes with adjusted  $P \leq 0.05$  and fold change  $> 2$  or  $< 0.5$  (compared to DMSO treatment) were considered to be significantly differentially expressed genes. Numbers next to the bars indicate the  $P$ -values. **B**) Expression pattern of differentially expressed Tartary buckwheat genes related to JA biosynthesis and signaling during *R. solani* infection, shown as a heatmap of  $\log_2FC$  at the 6-, 14-, and 22-h time points relative to the control samples. Red and blue indicate upregulation and downregulation, respectively. Intensity of the colors is proportional to the  $\log_2FC$ . TGL, triacylglycerol lipase; LOX, 13-lipoxygenase; AOS, allene oxide synthase; AOC, allene oxide cyclase; OPR, (9S,13S)-12-oxo-phytodienoic acid reductase; ACOX, acyl-CoA oxidase; ACAA, 3-oxoacyl-CoA thiolase; MEP, multifunctional protein; JAR1, JASMONATE RESISTANT 1/jasmonate-amino synthetase; JAZ, JA ZIM domain; COI1, CORONATINE INSENSITIVE 1; ERF, ETHYLENE-RESPONSIVE TRANSCRIPTION FACTOR; PR, PATHOGENESIS RELATED. **C**) Venn diagram showing the number of Tartary buckwheat genes commonly and uniquely differentially expressed during *R. solani* infection and MeJA treatment. The leaves of 21-d-old Tartary buckwheat seedlings were inoculated with mycelial disks subcultured on PDA medium for 6 (FT 6 h), 14 (FT 14 h), or 22 h (FT 22 h), or treated with 50  $\mu\text{M}$  MeJA for 1 (JA 1 h), 4 (JA 4 h), or 12 h (JA 12 h); the leaves were then harvested for transcriptome analysis. Three independent biological replicates ( $n = 10$  seedlings each) for each treatment were conducted. Genes with adjusted  $P \leq 0.05$  and fold change  $> 2$  or  $< 0.5$  (compared to DMSO treatment for JA treatment or noninoculated control samples for *R. solani* infection) were considered to be significantly differentially expressed genes and used for analysis. FT, *F. tataricum*; JA, jasmonic acid. **D**) Most significantly enriched KEGG metabolic pathways of JA-induced or repressed differentially expressed genes in Tartary buckwheat during *R. solani* infection. Numbers next to the bars indicate the  $P$ -values.

both *R. solani* infection and MeJA treatment remain unknown. Moreover, their involvement in disease resistance needs to be elucidated. In particular, it is necessary to find a suitable method to narrow down the number of candidate disease resistance genes. We thus turned to GWAS in combination with transcriptome analysis to mine for disease resistance genes. To this end, we measured the disease index of 320 Tartary buckwheat accessions collected worldwide (Supplemental Data Set 43). The coefficient of variation (CV) was ~65.6%, indicating that disease resistance is highly variable among Tartary buckwheat varieties, providing valuable genetic resources for cultivating varieties with high disease resistance. Then, using polymorphisms identified in our previous efforts to sequence the genome of these varieties (Zhang et al. 2021), we carried out GWAS to identify genomic regions significantly associated with *R. solani* resistance, using the disease index as phenotype (Supplemental Fig. S34). We identified a total of 122 significant single-nucleotide polymorphisms (SNPs) located on 7 out of the 8 chromosomes. We looked for candidate genes in 200 kb of flanking sequences on either side near each significant SNP, resulting in 16 genomic regions harboring 790 genes (Fig. 5A and Supplemental Data Set 44).

A KEGG analysis revealed that 14 candidate genes are involved in plant–pathogen interactions, confirming the reliability of the GWAS results (Supplemental Fig. S35). Among them, homologs of WRKY transcription factor gene (FtPinG0809055500) are important regulator of plant defense responses (Pandey and Somssich 2009). 3-Ketoacyl-CoA synthase (FtPinG0708058700) is a wax biosynthesis gene whose *Arabidopsis* homolog was shown to be involved in disease resistance (Weidenbach et al. 2014; Wang, Zhi, et al. 2019; Zhang, Zhang, et al. 2019). Homologs of LysM domain receptor–like kinase (FtPinG0100600300) are necessary in plant recognition of the fungal cell wall major component chitin (Wan et al. 2012; Ao et al. 2014; Paparella et al. 2014). Homologs of calcium-dependent protein kinase (FtPinG0100542000; Bundó and Coca 2016; Wei et al. 2016; Bundó and Coca 2017; Lu et al. 2020; Wu et al. 2021) are positive, while homologs of cyclic nucleotide–gated ion channel (FtPinG0100588800; Moeder et al. 2011; Wang, Liu, et al. 2019) are negative regulators of disease resistance. The identification of these plant–pathogen interaction–related genes confirm the reliability of the GWAS results and provide important clues for understanding the genetic architecture of disease resistance in Tartary buckwheat. In addition, as plant disease resistance is tightly associated with the content of secondary metabolites, which is greatly affected by the environment, we compared the above GWAS regions with our previous metabolic GWAS (mGWAS) data (Zhao et al. 2023). We observed an overlap between 5 regions associated with 3 disease resistance metabolites and disease index (Supplemental Data Set 45 and Fig. S36). The metabolites tangeretin (Liang et al. 2021), indole (Shen et al. 2018), and indole-3-carboxylic acid (Gamir et al. 2012; Pastor-Fernández et al. 2019) have been previously shown to be involved in plant disease resistance.

We integrated all GWAS results with the transcriptomes from *R. solani* inoculation and JA treatment to screen candidate disease resistance genes. We detected 106 genes located in 15 associated regions whose transcript levels respond to both *R. solani* infection and MeJA treatment (Fig. 5B and Supplemental Data Set 46). Among them, 49 genes were upregulated during *R. solani* infection and MeJA treatment. Most of these genes that have been previously shown increased the plant disease resistance in other plant species, including homologs of aspartic proteinase (FtASP, FtPinG0302743900; Xia et al. 2004; Prasad et al. 2009), alcohol dehydrogenase (FtADH1, FtPinG0302737400; Shi et al. 2017), calcium-dependent protein kinase (FtPinG0100542000; Bundó and Coca 2016; Wei et al. 2016; Bundó and Coca 2017; Lu et al. 2020; Wu et al. 2021), BTB/POZ domain-containing protein (FtPinG0607121100; Zhang, Gao, et al. 2019), cellulose synthase (FtCSLG2, FtPinG0404615400; Choe et al. 2021), and carboxylesterase (FtCES18, FtPinG0809058900; Ko et al. 2016). The upregulation of these JA–induced genes during *R. solani* infection might contribute to JA–induced disease resistance responses. Sixteen genes were downregulated during *R. solani* infection while upregulated after MeJA treatment. Most of these genes that were previously shown have disease resistance ability in other plant species, including homologs of an ABC transporter gene (FtPinG0404610000; Bienert et al. 2012; Sasse et al. 2016; Khare et al. 2017), E3 ubiquitin-protein ligase (FtPinG0404612300; Karki et al. 2021), ferredoxin (FtPinG0707939600; Huang et al. 2007; Ger et al. 2014; Wang et al. 2018; Cui et al. 2021), and glutamate receptor (FtPinG0708049000; Liu et al. 2021). The downregulation of these JA–induced resistance genes during *R. solani* infection might be necessary for pathogens to infect plant cells successfully. In summary, the majority of the overlapping genes obtained by GWAS and transcriptomics were related to disease resistance, suggesting that the combination of GWAS with transcriptome data can be an effective strategy for screening candidate disease resistance genes.

### JA–induced FtASP inhibits *R. solani* AG4-HGI 3 infection by suppressing fungal growth

To clarify the functions of candidate disease resistance genes and verify the efficiency of our strategy combining GWAS with transcriptomes in disease resistance gene screening, we chose candidate genes for experimental exploration: 5 genes identified by GWAS (FtASP, FtADH1, FtPG1, FtCES18, and FtCSLG2) that are significantly upregulated during *R. solani* infection and following MeJA treatment and 1 gene identified by GWAS (FtKCS11) that is significantly downregulated during *R. solani* infection but is upregulated following MeJA treatment (Fig. 5B). We heterologously expressed all genes individually in *Arabidopsis* and subjected their leaves to disease resistance assays (Supplemental Fig. S37). Five genes (FtASP, FtADH1, FtPG1, FtCES18, and FtKCS11) resulted in enhanced disease resistance (Figs. 6, S38, and S39). One gene

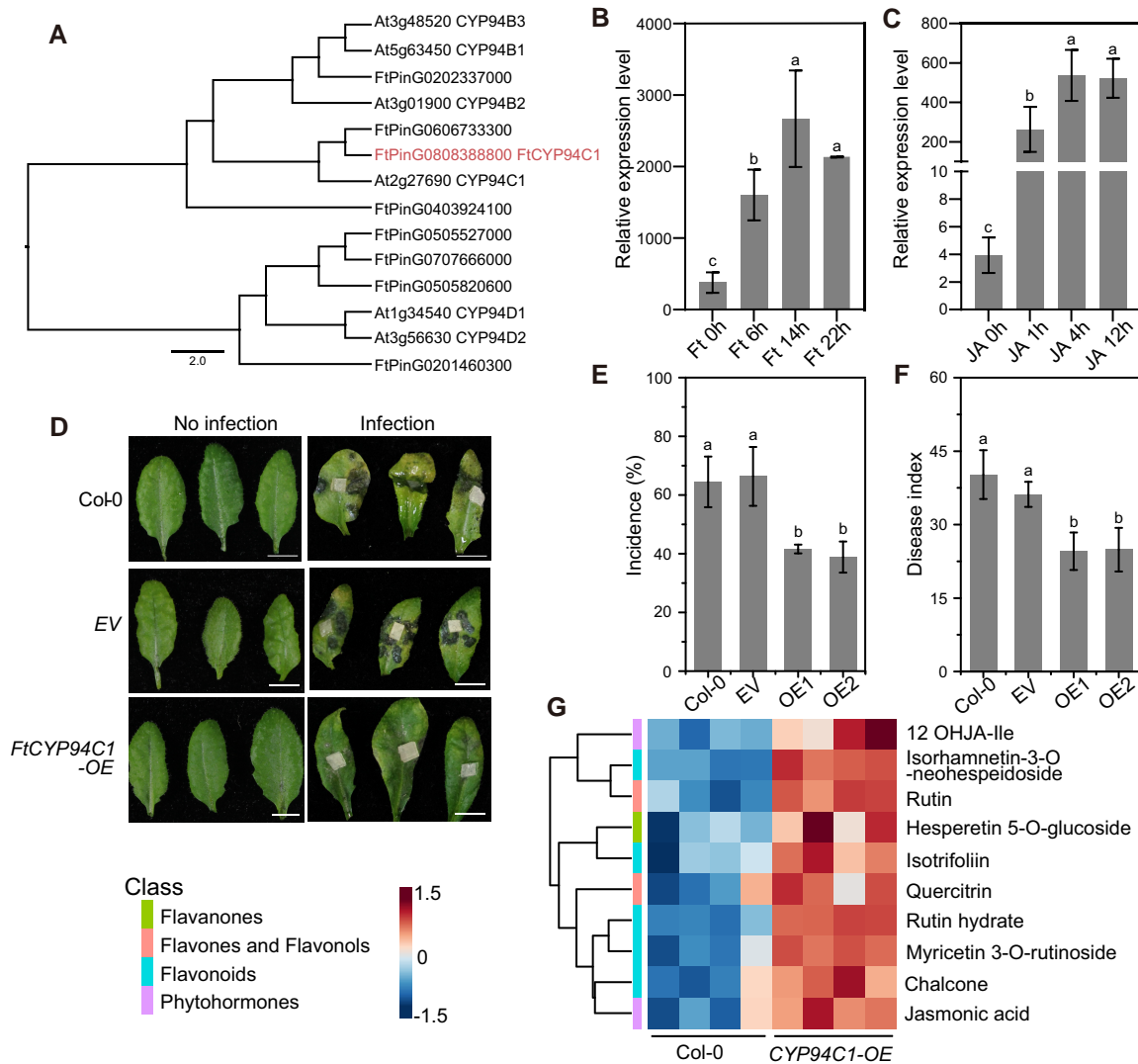


**Figure 4.** JA-induced *FtCYP94C1* improves disease resistance of Tartary buckwheat to *R. solani* AG4-HGI 3. **A)** Phylogenetic tree illustrating the relatedness of Tartary buckwheat CYPs (Ft) to *Arabidopsis* CYPs (Atxg). The full-length amino acid sequences were used for phylogenetic analysis based on the neighbor-joining method. Only a subset of CYPs with high amino acid similarity to *FtCYP94C1* is shown. The scale bar at the bottom represents the number of expected substitutions per site. Red represents *FtCYP94C1*. **B, C)** Relative *FtCYP94C1* expression levels during *R. solani* infection **B)** and MeJA treatment **C)**. For *R. solani* infection, the leaves of 21-d-old Tartary buckwheat seedlings were inoculated with mycelial disks subcultured on PDA medium for 6, 14, or 22 h **B)** or treated with 50  $\mu\text{M}$  MeJA for 1, 4, or 12 h **C)** and then collected for transcriptome analysis. Expression levels are estimated as FPKM values. Data show the arithmetic mean  $\pm$  SD from 3 biological replicates ( $n = 10$  seedlings each). Different letters indicate significant differences at adjusted  $P < 0.05$  (corrected using the Benjamini–Hochberg method). **D)** Phenotype of *Arabidopsis* lines heterologously expressing *FtCYP94C1* and infected with *R. solani* AG4-HGI 3. The detached leaves of 2-wk-old *Arabidopsis* seedlings were inoculated with subcultured mycelial disks for 2 d. The *Arabidopsis* leaves of wild-type (Col-0) or from lines transformed with the empty vector (EV) control were used as negative controls. The phenotypes were observed in leaves of 3 *Arabidopsis* seedlings ( $n = 3$ ). The experiments were performed 3 times using different batches of *Arabidopsis* seedlings. Photographs from 1 representative experiment are shown. Scale bars, 1 cm. **E, F)** Disease incidence **E)** and disease index **F)** of *Arabidopsis* lines heterologously expressing *FtCYP94C1* (OE1 and OE2) infected with *R. solani* AG4-HGI 3. Leaves were treated as above, and the disease index was evaluated 2 d later. Data show the arithmetic mean  $\pm$  SD from 3 biological replicates ( $n = 5$ ). Different letters indicate significant differences at  $P < 0.01$  (1-way ANOVA, Tukey's posttest). The experiment was performed 3 times using different batches of *Arabidopsis* seedlings with similar results. **G)** *Arabidopsis* lines heterologously expressing *FtCYP94C1* accumulate JA derivatives and flavonoids. Two-week-old *Arabidopsis* seedlings were used for metabolite analysis. Four independent biological replicates ( $n = 10$ ) for each treatment were conducted. Red and blue indicate upregulation and downregulation, respectively. Intensity of the colors is proportional to the metabolite content.

(*FtCSLG2*) showed suppressed disease resistance (Supplemental Figs. S38 and S39). Therefore, all genes tested in this assay changed plant disease resistance, confirming the high efficiency of our strategy combining GWAS with plant–

pathogen interaction and phytohormone-related transcriptomes for exploitation of disease resistance genes.

It is worth noting that *FtPinG0302743900*, encoding an aspartic protease (*FtASP*), 1 of the candidate proteins interacting



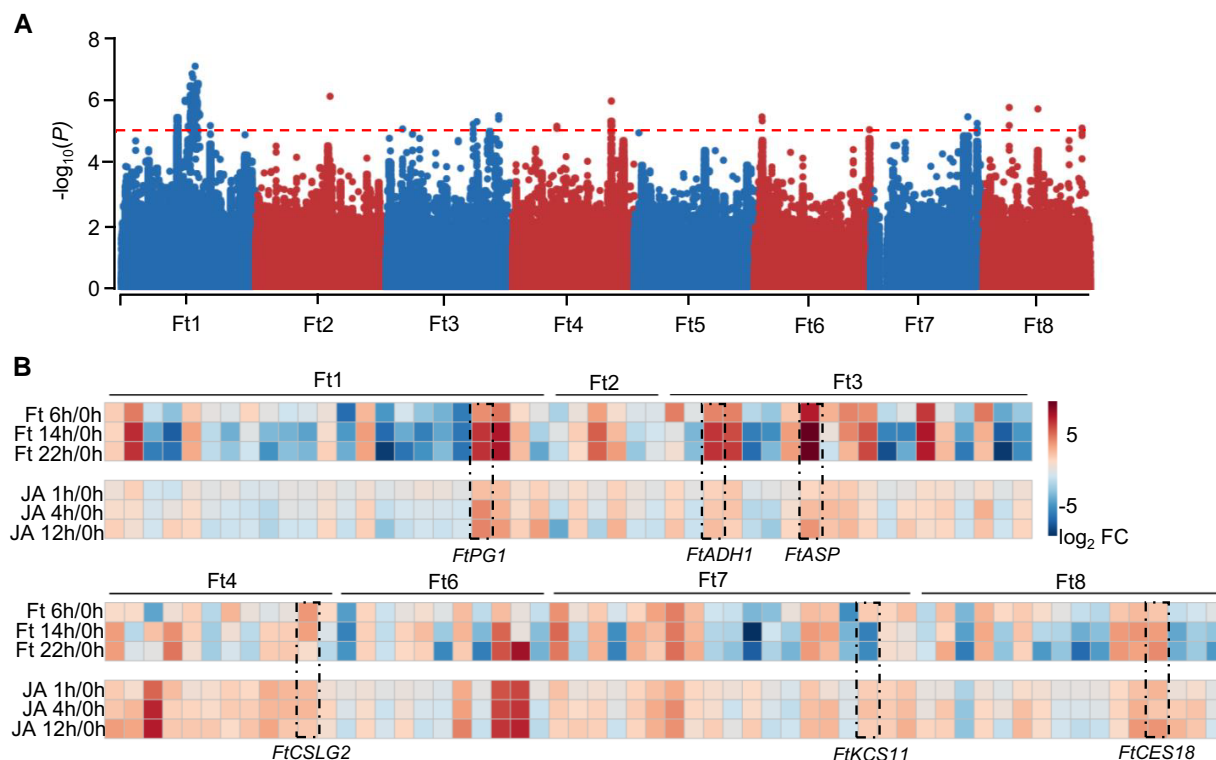


**Figure 5.** The integration of GWAS and transcriptomics identifies 106 genes associated with Tartary buckwheat disease resistance to *R. solani* AG4-HGI 3. **A**) Manhattan plot of the GWAS results using disease index in 320 Tartary buckwheat accessions as phenotype. Seven-day-old Tartary buckwheat seedlings were inoculated with a 50× diluted subcultured mycelial solution, and the disease index was evaluated 5 d later. The mean values of the disease index from 3 biological replicates ( $n = 10$ ) for each accession were used for GWAS analysis. The red dotted line represents the significance threshold. **B**) Heatmap representation of the expression pattern of GWAS-identified genes that were both differentially expressed during infection with *R. solani* (Ft; top) and following MeJA treatment (JA; bottom). The mean FPKM values of 3 biological replicates ( $n = 10$ ) during *R. solani* infection or MeJA treatment were used to calculate the relative expression level of these genes (shown as  $\log_2FC$  relative to noninfected for *R. solani* infection and untreated seedlings for MeJA treatment). Red and blue indicate upregulation and downregulation, respectively. Intensity of the colors is proportional to  $\log_2FC$ . Genes used in transgenic experiments are outlined with dotted lines. *FtPG1*, polygalacturonase like, FtPinG0100647900; *FtADH1*, alcohol dehydrogenase-like 1, FtPinG0302737400; *FtASP*, aspartic proteinase, FtPinG0302743900; *FtCSLG2*, cellulose synthase-like protein G2, FtPinG0404615400; *FtKCS11*, 3-ketoacyl-CoA synthase 11 like, FtPinG0708058700; *FtCES18*, probable carboxylesterase 18, FtPinG0809058900.

with the virulence protein RsYTHDC, showed the highest expression during *R. solani* inoculation and was significantly up-regulated following MeJA treatment and was also identified by GWAS. Haplotype analysis indicated that the 320 Tartary buckwheat accessions can be divided into 2 main haplotypes for this gene, with the C-haplotype exhibiting a higher disease resistance than the T-haplotype (Fig. 6A). Accessions with the C-haplotype were widely distributed, while those harboring the T-haplotype were mainly distributed in northern China (Supplemental Fig. S40). Reverse transcription quantitative PCR (RT-qPCR) analysis determined that *FtASP* expression is negatively correlated with the disease index in different Tartary buckwheat accessions, confirming the disease resistance ability of *FtASP* (Fig. 6B). The heterologous expression of *FtASP* in *Arabidopsis* had no effect on naïve plants but significantly improved their resistance to *R. solani* AG4-HGI 3 (Figs. 6, D and E, and S41 to S43). Moreover, the addition of recombinant purified full-length *FtASP* and its first half (Supplemental Fig. S44) inhibited the growth of *R. solani* AG4-HGI 3, while

the addition of the second half of *FtASP* did not affect fungal growth (Figs. 6F and S45). Previous work had indicated that aspartic proteases are involved in plant resistance to both bacterial and fungal pathogens (Xia et al. 2004; Prasad et al. 2009; Wang et al. 2022). We therefore speculate that *FtASP* is a vital component of resistance to *R. solani* in Tartary buckwheat and potentially other pathogens. However, a protease assay revealed that *FtASP* has no protease activity (Supplemental Fig. S46); rather, the N-terminal protein sequence GPLKFNNTLLSINKVSGSGTTI (amino acids 57 to 79) showed a high probability to be an antimicrobial peptide (Waghu and Idicula-Thomas 2020), suggesting that *FtASP* might not function as a protease but as an antimicrobial peptide.

## Discussion

*R. solani* is a destructive and widespread fungal pathogen with significant scientific and economic importance (Dean et al. 2012). A better understanding of its pathogenicity is

critical to develop effective disease resistance strategies. Isolates from some *R. solani* AGs (AG3, AG5, and AG8) exhibit a limited host range, while those in AG1 and AG2 can infect a broader spectrum of host plants (Wibberg et al. 2013). The universality and complexity of host range present great challenges for the study of the mechanisms underlying pathogenicity. At present, due to its economic importance, most research has concentrated on *R. solani* AG1-IA, the predominant causal agent of rice sheath blight disease, while the basis of pathogenicity of other isolates that infect other economically important crops has yet to be studied. Here, we demonstrated that a *R. solani* AG4 isolate (AG4-HGI 3), originally identified from Tartary buckwheat, could infect an extensive range of host plants, including plants in the Poaceae, Brassicaceae, and Leguminosae, representing a similar host range to that determined for AG1 (Wibberg et al. 2013). To investigate the genetic basis of its wide range of host plants, we sequenced and assembled the genome of *R. solani* AG4-HGI 3. Notably, we established that *R. solani* AG4-HGI 3 was a multinucleus isolate, with a variable number of nuclei number in a single cell. The specificities of this isolate bring great difficulties to genome assembly, resulting in the inability to reach chromosome-level scaffolding (Hane et al. 2014; Duan et al. 2022). The assembled genome of *R. solani* AG4-HGI 3 was larger than that of other *R. solani* isolates, which might be also due to the higher number of nuclei within a single cell (Takashima et al. 2018). Comparative genomic analysis showed that *R. solani* AG4-HGI 3 possessed abundant carbohydrate degradation-related genes and secreted proteins encoding genes, which might be associated with its extensive host range. Transcriptome analysis revealed that the expression of numerous genes in *R. solani* increased following 14 h of infection, with nearly half of CAZyme genes being upregulated at this time point, suggesting that this period may be necessary for *R. solani* AG4-HGI 3 infection and plant cell wall degradation. Similar results were previously obtained following infection of rice with *R. solani* AG1-IA, with most genes being differentially expressed at 18-h post-inoculation (Zheng et al. 2013). In addition, abundant pathogenesis-related genes were upregulated during *R. solani* infection, including some encoding key effectors previously identified as essential for *R. solani* pathogenesis such as proteins with NUDIX, NACHT, or BTB domains (Li, Guo, et al. 2021; Li, Li, et al. 2021). Our findings therefore add to the knowledge necessary to help reveal the genetic and biological mechanisms during *R. solani* pathogenicity.

Previous research indicated that genes involved in plant hormone signaling are differentially expressed during *R. solani* infection (Zrenner et al. 2021) and elevating JA levels enhanced rice resistance against *R. solani* (Taheri and Tarighi 2010). However, how JA participates in the regulation of plant disease resistance has yet to be fully uncovered. Here, we identified numerous JA-induced genes as being involved in the Tartary buckwheat response to *R. solani* infection. Among them, *FtCYP94C1* was a negative regulator of the typical JA signaling pathway (Koo et al. 2011; Heitz et al. 2012; Koo et al.

2014), while a positive modulator of disease resistance-related flavonoid biosynthesis (Poudel et al. 2019). Combined with the enhanced disease resistance and metabolomic alterations of *Arabidopsis* lines heterologously expressing this gene, we suggest that *FtCYP94C1* enhances disease resistance of Tartary buckwheat by regulating flavonoid biosynthesis rather than via the typical JA signaling pathway. In addition, we detected several JA-induced genes that were involved in Tartary buckwheat disease resistance. However, due to the complexity of plant disease, there is no universal relationship between classes of genes and pathogen resistance. For instance, some aspartic proteases (Xia et al. 2004; Prasad et al. 2009), cellulose synthases (Choe et al. 2021), alcohol dehydrogenases (Shi et al. 2017), and carboxylesterases (Ko et al. 2016) enhance disease resistance, while others suppress disease resistance (Hernández-Blanco et al. 2007; Liu et al. 2014; Wang et al. 2022). Here, we showed that the protease-like protein *FtASP* exhibited no aspartic protease activity, although it did inhibit fungal growth through the activity of its N-terminal region. As some N-terminal peptides were found to exert antibacterial function and exhibit a wide spectrum of antimicrobial activity (Zhao et al. 2020), we speculate that *FtASP* may function as an antimicrobial peptide to inhibit *R. solani* growth. In summary, the exploration of these plant defense-related genes will enrich our understanding of how plant hormones regulate plant disease resistance, with implications for accelerating the molecular breeding of disease-resistant varieties of economically important crop species.

The exploitation of genetic variation in natural population via GWAS is an effective strategy for the identification of disease resistance genes (Kankanala et al. 2019; Molla et al. 2020). However, insufficient marker density, linkage disequilibrium, and high false-positive rates represent a severe challenge for functional validation of candidate resistance genes (Shu et al. 2021). The combination of GWAS and transcriptome analysis, as employed here, can overcome these limitations and hence accurately identify critical candidate resistance genes. Although the integration of GWAS and transcriptome analysis has been used to identify disease resistance genes in the past (Wen et al. 2018; Yao et al. 2020; Shu et al. 2021), most of these studies only explored comparisons between the transcriptomes of resistant and susceptible plants. As large-scale transcriptome data are only available in a few major crops, some systematically well-developed analysis methods (such as summary data-based Mendelian randomization [SMR]; Zhu et al. 2016) could not be widely used to integrate GWAS and RNA-seq data. Here, by combining the results from *R. solani* inoculation and JA-mediated transcriptome analyses, we determined that the JA signaling gene *FtCYP94C1* enhanced resistance to *R. solani* AG4-HGI 3 in Tartary buckwheat apparently by promoting the biosynthesis of disease resistance-related flavonoids. By combining transcriptomes obtained during the plant-pathogen interaction and following JA treatment with GWAS, we identified 106 candidate genes that may be associated with disease resistance, which we argue that it is an efficient approach to greatly reduce the number of

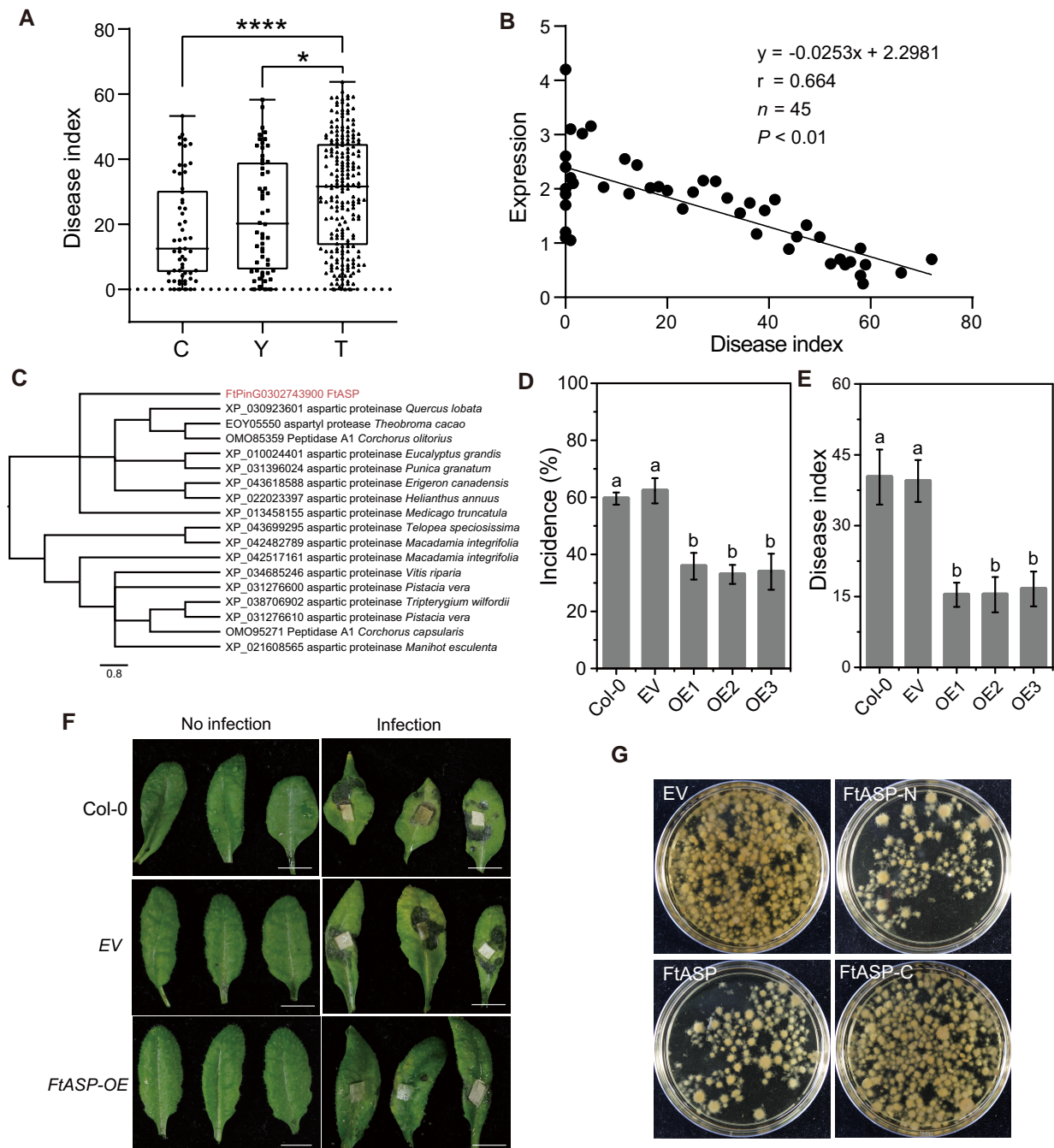


**Figure 6.** JA-induced FtASP improves disease resistance of Tartary buckwheat to *R. solani* AG4-HGI 3. **A**) Box plots of the disease index in Tartary buckwheat accessions harboring the C-haplotype (53 accessions), the T-haplotype (210 accessions), and the Y(C/T)-haplotype (54 accessions). The data are based on the mean disease index values from 3 biological replicates ( $n = 10$ ) for each accession.  $*P < 0.05$  and  $****P < 0.0001$ , as calculated using 2-tailed Student's *t*-test. **B**) Relative FtASP expression levels in different Tartary buckwheat accessions. The mean values from 3 biological replicates ( $n = 10$ ) for each accession were used for analysis. The formula, *r*-value, and *P*-value of the regression line were shown. **C**) Phylogenetic tree for ASP proteins using full-length amino acid sequences from Tartary buckwheat (FtASP) and other plants. The phylogenetic tree was reconstructed using the neighbor-joining method. Only a subset of ASPs with high amino acid similarity to FtASP is shown. The scale bar at the bottom represents the number of expected substitutions per site. Red represents FtASP. **D, E**) Incidence **D**) and disease index **E**) of *Arabidopsis* lines heterologously expressing FtASP (OE1, OE2, and OE3) infected with *R. solani* AG4-HGI 3. The detached leaves of 2-wk-old *Arabidopsis* seedlings were inoculated with the subcultured mycelial disks, and the disease index was evaluated after 2 d. The *Arabidopsis* leaves of wild-type (Col-0) and lines transformed with the empty vector (EV) control were used as negative controls. Data show the arithmetic mean  $\pm$  SD from 3 biological replicates ( $n = 5$  seedlings each). Different letters indicate significant differences at  $P < 0.01$  (1-way ANOVA, Tukey's posttest). The experiment was performed 3 times using different batches of *Arabidopsis* seedlings with similar results. **F**) Phenotype of *Arabidopsis* lines heterologously expressing FtASP infected with

(continued)



candidate genes identified through each separate analysis and likely reduces the false-positive identification of candidate resistance genes. In conclusion, our strategy efficiently identified key components of the *R. solani* pathogenicity response in Tartary buckwheat, which can be investigated in other crops susceptible to this strain with broad host range. Further, multiomic analysis such as that presented in this work will enhance the understanding of pathogenicity of other diseases in other agronomically important crop species, thus streamlining the identification of candidate resistance genes for molecular breeding of disease resistance.

In summary, our study demonstrated that *R. solani* AG4-HGI 3 exhibited a larger genome size and harbored more protein-coding genes than most other *R. solani* isolates. Moreover, the expansion of pathogenicity genes might be responsible for the broad host range of *R. solani* AG4-HGI 3. In addition, some jasmonate-induced genes in Tartary buckwheat enhanced the resistance to *R. solani*. These results will enrich the knowledge of pathogenicity in *R. solani* and hence accelerate the molecular breeding of resistant varieties in economically important crops.

## Materials and methods

### *R. solani* AG4-HGI 3 isolates and culture conditions

The strain *R. solani* AG4-HGI 3 was isolated from Tartary buckwheat (*F. tataricum* [L.] Gaertn.) in the field and characterized as AG4-HGI 3 (Li, Zhang, et al. 2021). This fungal isolate causes sunken lesions and dark brown symptoms on the root and stem of Tartary buckwheat. The cultures of *R. solani* AG4-HGI 3 were revived from stock cultures maintained at  $-80^{\circ}\text{C}$  by placing mycelial disks on fresh potato dextrose agar (PDA) for 5 d, at  $28^{\circ}\text{C}$ , in the dark. The isolates were then subcultured on fresh PDA for 5 d or potato dextrose broth (PDB) for 3 d, at  $28^{\circ}\text{C}$ , in the dark before being used for experiments. Nuclei in hyphae were stained using DAPI according to the method described previously (Li, Guo, et al. 2021; Li, Li, et al. 2021).

### Genome assembly and comparative genomics

The pathogen subcultured on PDB medium was used to extract the genomic DNA via a Fungal DNA Kit (D3390-02, Omega BioTek, Norcross, USA), according to the manufacturer's instructions. Purified DNA was quantified on a TBS-380 fluorometer (Turner BioSystems Inc., Sunnyvale, CA, USA). The genome was sequenced using PacBio Sequel Single Molecule Real Time (SMRT) and Illumina sequencing platforms at Shanghai Majorbio Biopharm Biotechnology Co., Ltd., China. The genome

size and heterozygosity of *R. solani* AG4-HGI 3 were estimated based on the distribution of 17-mers using Meryl (Rhie et al. 2020) and GenomeScope v1.0 (<https://github.com/schatzlab/genomescope>; 2017). The Illumina short reads were quality controlled using fastp v0.23.0 (<https://github.com/OpenGene/fastp>; Chen et al. 2018). The PacBio long reads were assembled using CANU v1.7 (<http://canu.readthedocs.io/en/latest/>; Koren et al. 2017). The assembled contigs were corrected and polished through Illumina short reads using RACON (<https://github.com/lbcb-sci/racon>; Vaser et al. 2017). For annotation, the open reading frames (ORFs) of genes were predicted using Maker 2 v2.31.9 (<http://www.yandell-lab.org/software/maker.html>; Cantarel et al. 2008) and annotated through alignment against the NR, Swiss-Prot, Pfam, GO, COG, and KEGG databases using the sequence alignment tools BLAST, Diamond v0.8.35 (<https://github.com/bbuchfink/diamond>; Buchfink et al. 2015) and HMMER v3.1b2 (<http://www.hmmer.org/>; Eddy 1998). The rRNA and tRNA in the genome were predicted using Barrnap 0.4.2 (<https://github.com/tseemann/barrnap>; Seemann 2014) and tRNAscan-SE v 1.3.1 (<http://lowelab.ucsc.edu/tRNAscan-SE/>; Lowe and Eddy 1997). Repeat regions were masked using RepeatMasker v4.0.7 (<http://www.repeatmasker.org/RepeatMasker/>; Tarailo-Graovac and Chen 2009). Predicted secreted proteins were defined as proteins with a signal peptide using SignalP v5.0 (<https://services.healthtech.dtu.dk/service.php?SignalP-5.0>; Almagro Armenteros et al. 2019) and no transmembrane domains using TMHMM v2.0 (<https://services.healthtech.dtu.dk/service.php?TMHMM-2.0>). CAZymes were identified by applying dbCAN2 (<https://bcb.unl.edu/dbCAN2/>; Zhang, Yohe, et al. 2018; Zhang, Logacheva, et al. 2018). The Pathogen Host Interaction database (PHI-base, <http://www.phi-base.org>; Winnenburger et al. 2006) was used to find sequence homology relative to known virulence and pathogenicity markers. The effector proteins were predicted using effectorP v3.0 (<https://effectorp.csiro.au/>; Sperschneider and Dodds 2022).

OrthoMCL v1.4 (<http://www.orthomcl.org>; Li et al. 2003) was used to construct orthologous gene families. MUSCLE v3.7 (<http://drive5.com/muscle>; Edgar 2004) was used to align single-copy orthologous genes. RAXML v8.0.19 (<https://cme.h-its.org/exelixis/web/software/raxml>; Stamatakis 2014) was used to construct the maximum likelihood-based phylogenetic tree by employing sequence alignments with *M. oryzae* as the outgroup. The unfiltered alignment and phylogenetic tree of are provided as Supplemental Files 1 and 2. CAFÉ v1.6 (<https://sourceforge.net/projects/cafehahnlab>) was used to determine the expansion and contraction of orthologous gene families. Synteny was analyzed using MUMmer v3

(Figure 6. Continued)

*R. solani* AG4-HGI 3. Leaves were treated as above. Phenotypes were observed from the leaves of 3 *Arabidopsis* seedlings ( $n = 3$ ). The experiment was performed 3 times using different batches of *Arabidopsis* seedlings. Photographs from 1 representative experiment are shown. Scale bars, 1 cm. **G**) Inhibitory effect of recombinant FtASP (1 to 225), FtASP-N (1 to 112), and FtASP-C (113 to 225) proteins on the growth of *R. solani* AG4-HGI 3. Purified recombinant proteins were added to PDB medium preinoculated with *R. solani* AG4-HGI 3. The effects of each recombinant protein were evaluated after culture for 2 d. The phenotypes were observed in 3 biological replicates ( $n = 3$ ). The experiment was performed 3 times using different batches of purified recombinant proteins with similar results. Photographs from 1 representative experiment are shown.

(<https://mummer.sourceforge.net/>; Kurtz et al. 2004), and the Circos plot was drawn using shinyCircos (<https://github.com/YaoLab-Bioinfo/shinyCircos>; Yu et al. 2018). Genes were annotated with GO annotation using InterProScan v5.53 to 87.0 (<http://www.ebi.ac.uk/interpro/search/sequence/>; Jones et al. 2014).

### Transcriptome analysis

The surface-sterilized Tartary buckwheat seeds were grown for 21 d at 22 °C (day/night) under long-day conditions (16-h light/8-h dark). For the transcriptome analysis of the *R. solani*–Tartary buckwheat interaction, mycelial disks subcultured on PDA medium were used to infect the leaves of Tartary buckwheat (Chuanqiao 1#) seedlings for 6, 14, and 22 h. For MeJA treatment, leaves of Tartary buckwheat seedlings were treated with 50  $\mu\text{M}$  MeJA (W341002, Sigma-Aldrich, Taufkirchen, Germany) for 1, 4, or 12 h. Three independent biological replicates for each treatment were conducted. Each replicate was obtained by pooling samples from 10 seedlings. Tartary buckwheat leaves were flash-frozen in liquid nitrogen and ground to a fine powder. Total RNA was extracted with TRIzol reagent (15596026, Invitrogen, Carlsbad, USA); genomic DNA was removed using DNase I (2270A, TaKara, Kusatsu, Japan). RNA-seq sequencing libraries were prepared using a TruSeq RNA sample preparation Kit (RS-122-2001) from Illumina (San Diego, USA) and sequenced with an Illumina HiSeq X Ten/Nova Seq 6000 instrument. Raw paired-end reads were trimmed and quality controlled by SeqPrep (<https://github.com/jstjohn/SeqPrep>) and Sickle (<https://github.com/najoshi/sickle>) with default parameters. Then, the clean reads were aligned to the reference genome of *R. solani* AG4-HGI 3 and Tartary buckwheat (HERA) with orientation mode using HISAT2 (<http://ccb.jhu.edu/software/hisat2/index.shtml>) software (Kim et al. 2015), respectively. The mapped reads for each sample were assembled by StringTie (<http://ccb.jhu.edu/software/stringtie/index.shtml?t=example>) in a reference-based approach (Pertea et al. 2015). The expression level of each transcript was calculated according to the fragments per kilobase of transcript per million fragments mapped (FPKM) method using RSEM (<http://deweylab.biostat.wisc.edu/rsem/>; Li and Dewey 2011). Differential expression analysis was performed using DESeq2 (Love et al. 2014), DEGseq (Wang et al. 2010) and EdgeR (Robinson et al. 2010). Genes with adjusted  $P \leq 0.05$  (corrected using the Benjamini–Hochberg method) and fold change  $> 2$  or  $< 0.5$  (compared to DMSO treatment for MeJA treatment and compared to noninoculated control samples for *R. solani* infection) were considered to be significantly differentially expressed genes. Functional enrichment of these differentially expressed genes was analyzed using the GO and KEGG databases.

### Recombinant protein purification and protease activity assay

Full-length cDNAs of *RsYTHDC*, *RsDAD*, *FtASP*, *FtASP-N*, and *FtASP-C* were amplified and inserted into the pET-28a

expression vector. Recombinant proteins were produced in *Escherichia coli* BL21 (DE3) cells (CD601-02, TransGen, Beijing, China) with 0.1 mM isopropyl- $\beta$ -D-1-thiogalactopyranoside (IPTG, I6758, Sigma-Aldrich, Taufkirchen, Germany) at 28 °C for 12 h. After sonication (200 W, 0 °C, 30 min; ultrasound for 5 s every 10 s), the crude extracts were centrifuged at 12,000  $\times g$  for 10 min, at 4 °C. Each supernatant was then purified using Ni-NTA Agarose (30210, Qiagen, Hilden, Germany). Immunoblotting of His-*RsYTHDC*, His-*RsDAD*, and His-*FtASP* was performed with anti-His (1:2,000; CW0286, CWBIO, Beijing, China) antibody. The molecular weight was marked using Rainbow Prestained Broad Molecular Weight Protein Marker (RTD6106, Real-Times Biotechnology Co., Ltd., Beijing, China). Protease activity was assessed using an EnzChek Protease Assay Kit (E6639, Invitrogen, Carlsbad, USA) following the manufacturer's instructions. The Endoproteinase Asp-N sequencing grade (ENDOARGS-RO, Roche Diagnostics GmbH, Mannheim, Germany) was used as a positive control. Three biological replicates were conducted, and the experiments were performed 3 times. Primer sequences are listed in Supplemental Data Set 47. The antimicrobial peptide was predicted using CAMP ([www.camp.bicnirrh.res.in](http://www.camp.bicnirrh.res.in); Waghu and Idicula-Thomas 2020).

### Subcellular localization of *RsYTHDC* and *RsDAD*

Full-length cDNAs of *RsYTHDC* and *RsDAD* were amplified and inserted into the pCambia1300-GFP vector. p2300-35s-H2B-mCherry was used as a nuclear marker. The plasmid was transferred into *N. benthamiana* leaves using *Agrobacterium* (*Agrobacterium tumefaciens*) strain GV3101-mediated transient infiltration (Wang et al. 2023). Subcellular localization was observed using a laser scanning confocal microscope (Zeiss LSM900) with the wavelengths of 488 (excitation)/500 to 530 nm (emission) for GFP and 561 (excitation)/590 to 640 nm (emission) for mCherry. Primer sequences are listed in Supplemental Data Set 47.

### Pull-down experiments and mass spectrometry

Pull-down and mass spectrometry assays were performed as described with some modifications (Brymora et al. 2004). Recombinant His-*RsYTHDC* and His-*RsDAD* proteins were used as bait. Total protein from Tartary buckwheat seedling was used as prey. The bait proteins were mixed with soluble protein extracts from Tartary buckwheat seedlings for 2 h at 4 °C and then immobilized on a Ni-NTA Agarose (30210, Qiagen, Hilden, Germany). Weakly bound proteins were removed by washing 3 times with wash buffer (10 mM phosphate-buffered saline [PBS pH 8.0], 20 mM imidazole, and 0.005% [ $v/v$ ] Tween 20). After elution with elution buffer (10 mM PBS, pH 8.0, and 250 mM imidazole), the supernatants were subjected to 10% SDS–PAGE followed by Coomassie Brilliant Blue staining. The gel was excised, tryptic digest, and subjected to LC-MS/MS analyzed by Shanghai Luming Biological Technology Co., Ltd. (Shanghai, China) according to methods described elsewhere (Qin et al. 2019).

### BiFC assay

Full-length cDNA of *FtSHMT* was amplified and inserted into the pSPYNE-35S vector. Full-length cDNA of *RsDAD* was amplified and inserted into the pSPYCE-35S vector. The constructs were introduced into *N. benthamiana* leaves using *Agrobacterium* (strain GV3101)-mediated infiltration. Fluorescence was observed using a laser scanning confocal microscope (Zeiss LSM900). Primer sequences are given in [Supplemental Data Set 47](#).

### Generation of transgenic lines and plant growth

Total RNA was extracted by using an RNAPre Pure Plant Plus kit (DP441, Tiangen, Beijing, China); first-strand cDNA was synthesized with a HiScript III RT SuperMix for qPCR (R323-01, Vazyme, Nanjing, China). The coding sequence was cloned into pCAMBIA-1307. The *N. benthamiana* and Tartary buckwheat transient expression and the *Arabidopsis* (*Arabidopsis thaliana*) overexpression lines were conducted and generated by *A. tumefaciens* (strain GV3101)-mediated transformation, respectively ([Clough and Bent 1998](#); [Wang et al. 2023](#)). Three biological replicates were conducted, and the experiments were performed 3 times. Protein accumulation in *N. benthamiana* leaves was analyzed by immunoblotting with an anti-MBP (1:2,000; CW0288M, CWBIO, Beijing, China) antibody. Relative expression levels of *Arabidopsis* heterologous expression lines were analyzed by RT-qPCR. Three biological replicates were conducted, and the experiments were performed 3 times. Primer sequences are given in [Supplemental Data Set 47](#). The T-DNA insertion mutants *aoc4* (SALK\_124897C) and *jar1* (SALK\_030821C) T-DNA were obtained from Arashare. The *myc2 myc3 myc4* triple mutant was described previously ([Fernández-Calvo et al. 2011](#)). All *Arabidopsis* genotypes were grown at 22 °C (day/night) under long-day conditions (16-h light/8-h dark). The phylogenetic tree of CYPs and ASPs was conducted using MEGAX based on the neighbor-joining method ([Saitou and Nei 1987](#); [Kumar et al. 2018](#)). The unfiltered alignment and phylogenetic tree are provided as [Supplemental Files 3 to 6](#).

### Treatment with phytohormones

For Tartary buckwheat treated with different phytohormones, 7-d-old Tartary buckwheat seedlings were pretreated with SA (1 mM, S7401, Sigma-Aldrich, Taufkirchen, Germany), MeJA (50  $\mu$ M), GA (100  $\mu$ M, 48870, Sigma-Aldrich, Taufkirchen, Germany), ethephon (1 mM, C0143, Sigma-Aldrich, Taufkirchen, Germany), or DMSO (negative control) for 3 h. Phenotypes were observed 3 d after onset of *R. solani* AG4-HGI 3 infection. Three biological replicates were conducted and the experiments were performed 3 times.

For *Arabidopsis* mutants treated with JA, the detached leaves of 2-wk-old *Arabidopsis* seedlings were pretreated with 50  $\mu$ M MeJA or DMSO (negative control) for 3 h and then inoculated with subcultured mycelial disks for 2 d.

Wild-type (Col-0) seedlings were used as negative control. Three biological replicates were conducted, and the experiments were performed 3 times.

### Metabolome analysis of *FtCYP94C1* overexpressing *Arabidopsis*

Two-week-old *Arabidopsis* seedlings were used to conduct a widely targeted metabolite analysis ([Want et al. 2010](#)). Four independent biological replicates for each treatment were conducted. Each replicate was obtained by pooling samples from 10 seedlings. Whole freeze-dried seedlings were ground and extracted with prechilled 80% (*v/v*) methanol/water. Following centrifugation at 15,000  $\times$  g at 4 °C for 20 min, the supernatants were analyzed by using an ExionLC AD system (SCIEX) coupled with a QTRAP 6500+ mass spectrometer (SCIEX) by Novogene Co., Ltd. (Beijing, China). The analytical conditions were as follows: column, Xselect HSS T3 (2.5  $\mu$ m, 2.1  $\times$  150 mm); Solvent A, 0.1% (*v/v*) formic acid water, and Solvent B, 0.1% (*v/v*) formic acid acetonitrile. The gradient program was as follows: 2% B, 2 min; 2% to 100% B, 15.0 min; 100% B, 17.0 min; 100% to 2% B, 17.1 min; 2% B, 20 min. The QTRAP 6500+ mass spectrometer was operated in positive/negative polarity modes with curtain gas of 35 psi, collision gas of medium, ionspray voltage of 5,500 V for positive and -4,500 V for negative, temperature of 550 °C, and ion source gas of 1:60.

Qualitative analysis was performed using multiple reaction monitoring (MRM) based on the Novogene database. The data files generated by HPLC-MS/MS were processed with SCIEX OS v1.4 to integrate and correct the peaks. The area of each peak represents the relative content of the corresponding metabolite. The metabolites were annotated using the KEGG database (<http://www.genome.jp/kegg/>), HMDB database (<http://www.hmdb.ca/>), and Lipidmaps database (<https://www.lipidmaps.org/>). Principal components analysis (PCA), partial least squares discriminant analysis (PLS-DA), and univariate analysis (*t*-test) were performed to identify the differentially abundant metabolites. The metabolites with VIP (variable importance for the projection) > 1, *P* < 0.05, and  $|\log_2 FC| \geq 1$  were considered to be differentially abundant.

### Flavonoids content analysis of *Arabidopsis* mutants

Flavonoid contents were analyzed according to the method described previously ([Zhang et al. 2021](#); [He et al. 2022](#)). Two-week-old *Arabidopsis* seedlings were freeze-dried and ground. The powder was extracted with prechilled 80% (*v/v*) methanol/water. The supernatant was analyzed by LC-MS (Agilent G6500 Series HPLC-QTOF). The content of flavonoids was calculated by comparing the HPLC peak area with authentic standards (Sigma-Aldrich, Taufkirchen, Germany). Three biological replicates were conducted, and each replicate was obtained by pooling samples from ten seedlings. The experiments were performed 3 times.



## Screening candidate host plants and disease resistance evaluation

For *R. solani* and Tartary buckwheat interaction, Tartary buckwheat seeds were germinated in petri plates containing wet filter paper at 22 °C. Seven days after germination, the seedlings were inoculated with 50× diluted subcultured mycelial solution for 5 d. Three biological replicates using 10 seedlings each were conducted. For validation of candidate virulence genes, detached transiently expressing *N. benthamiana* leaves were inoculated with subcultured mycelial disks for 2 d. Three biological replicates were conducted, and the experiments were performed 3 times. For the *R. solani*–*Arabidopsis* interaction, detached leaves of 2-wk-old *Arabidopsis* seedlings were inoculated with subcultured mycelial disks for 2 d. Three biological replicates were conducted, and the experiments were performed 3 times. For *R. solani* inoculation of other candidate host plant species, detached leaves of the appropriate size were inoculated with subcultured PDA mycelial disks. Plants inoculated with PDA or PDB medium without fungus were used as negative controls. Relative pathogen biomass was analyzed by measuring the abundance of the pathogen using qPCR of the internal transcribed spacer (ITS) region and normalized by plant biomass according to the method described previously (Wallon et al. 2020). Three biological replicates were conducted, and the experiments were performed 3 times. Primer sequences are listed in [Supplemental Data Set 47](#). Disease index evaluation, 3,30-diaminobenzidine (DAB) staining, and malondialdehyde (MDA) content analysis were conducted as previously described (Park et al. 2008; Bach-Pages and Preston 2018; Yin et al. 2020). Three biological replicates were conducted and the experiments were performed 3 times.

## Genome-wide association analysis

The resequencing data of 320 Tartary buckwheat accessions were obtained from published work (Zhang et al. 2021). GWAS was conducted using the method previously illustrated in Zhang et al. (2021). Briefly, the sequenced reads of Tartary buckwheat accessions were mapped to the reference genome of Tartary buckwheat (HERA; Zhang et al. 2017) using BWA-MEM (Li 2013). SNP calling was performed using the GATK pipeline (McKenna et al. 2010). After filtering (Quality > 30.0, Quality by Depth > 5.0, Fisher Strand < 60.0, and Depth > 5), a total of 1,095,350 high-quality SNPs (MAF > 0.05 and missing rate < 0.01) for 320 accessions were used to perform GWAS. The algorithm Efficient Mixed-Model Association eXpedited (EMMAX) was used to conduct all associations (Kang et al. 2010), with a significance threshold set to  $P = 1 \times 10^{-5}$ .

## Statistical analysis

Data of gene relative expression levels and disease index are shown as means ± SD. Significant differences were assessed using chi-square tests, 2-tailed Student's *t*-tests, 1-way and 2-way analysis of variance (ANOVA,  $P = 0.01$ ) performed

by SPSS22 software (SPSS, Chicago, IL, USA). Statistical data are provided as [Supplemental Data Set 48](#).

## Accession numbers

The genome sequencing data of this project are available from the National Center for Biotechnology Information under BioProject ID PRJNA917065. The raw transcriptome data of this project are available from the public database National Center for Biotechnology Information under BioProject ID PRJNA917064. The mass spectrometry proteomics data are available from the ProteomeXchange Consortium via the PRIDE partner repository with the data set identifier PXD041641. The metabolome data are available from the CNCB under BioProject ID PRJCA016408.

## Author contributions

M.Z. designed and managed the project. M.Z., A.R.F., M.A.C., and M.I.G. organized the funding for this research. J.C., B.X., and M.Z. provided the genetic materials. Y.H., K.Z., C.G., M.H., Y.S., and C.C. performed data analysis and figure design. Y.H., S.L., X.L., H.Z., X.H., Z.K., Y.F., W.L., G.L., O.L., and Y.C. performed most of the experiments. Y.H., K.Z., A.R.F., M.A.C., M.I.G., and M.Z. wrote the manuscript. All authors read and approved the manuscript.

## Supplemental data

The following materials are available in the online version of this article.

**Supplemental Figure S1.** Phenotypes of crops inoculated with *R. solani* AG4-HGI 3.

**Supplemental Figure S2.** DAPI staining of nuclei in *R. solani* AG4-HGI 3 hyphae.

**Supplemental Figure S3.** K-mer analysis for estimating the genome size of *R. solani* AG4-HGI 3.

**Supplemental Figure S4.** Correlation between the protein-coding gene number and the genome size using linear regression analysis.

**Supplemental Figure S5.** Circos plot showing the distribution of genes (I), transposons (II), CAZymes (III), secreted proteins (IV), effectors (V), virulence genes (VI), the duplicated genes based on BUSCO (VII), and the syntenic relationship (inner Circos).

**Supplemental Figure S6.** Circos plot showing the syntenic relationship between genomes of different isolates of *R. solani*.

**Supplemental Figure S7.** The most significantly enriched GO terms in contracted gene families.

**Supplemental Figure S8.** Correlation between genome size and the number of pathogenicity genes using linear regression analysis.

**Supplemental Figure S9.** Phenotype of Tartary buckwheat seedlings inoculated with *R. solani* AG4-HGI 3.

**Supplemental Figure S10.** The most significantly enriched GO terms of upregulated genes in *R. solani* AG4-HGI 3 during infection of Tartary buckwheat.

**Supplemental Figure S11.** The most significantly enriched GO terms of expanded gene families with upregulated expression (up) or downregulated expression (down) in *R. solani* AG4-HGI 3 during infection of Tartary buckwheat.

**Supplemental Figure S12.** The most significantly enriched KEGG metabolic pathways of expanded gene families (up, upregulated expression; down, downregulated expression) in *R. solani* AG4-HGI 3 during infection of Tartary buckwheat.

**Supplemental Figure S13.** The most significantly enriched GO terms of contracted gene families with upregulated expression (up) or downregulated expression (down) in *R. solani* AG4-HGI 3 during infection of Tartary buckwheat.

**Supplemental Figure S14.** The most significantly enriched KEGG metabolic pathways of contracted gene families (up, upregulated expression; down, downregulated expression) in *R. solani* AG4-HGI 3 during infecting Tartary buckwheat.

**Supplemental Figure S15.** Immunoblot with anti-MBP antibody to detect virulence proteins following transient expression in *N. benthamiana* leaves.

**Supplemental Figure S16.** Phenotypes observed on *N. benthamiana* leaves transiently expressing virulence genes.

**Supplemental Figure S17.** Relative pathogen biomass of *R. solani* AG4-HGI 3 infecting *N. benthamiana* leaves transiently expressing virulence genes.

**Supplemental Figure S18.** MDA content of *N. benthamiana* leaves transiently expressing virulence genes and infected with *R. solani* AG4-HGI 3.

**Supplemental Figure S19.** Subcellular localization of RsYTHDC and RsDAD.

**Supplemental Figure S20.** Immunoblot analysis with anti-His antibody to detect the purified recombinant His-RsYTHDC and His-RsDAD.

**Supplemental Figure S21.** BiFC assay showing interactions between FtSHMT and RsDAD in *N. benthamiana* leaf epidermal cells.

**Supplemental Figure S22.** The most significantly enriched GO terms of different expressed genes in Tartary buckwheat during infection by *R. solani* AG4-HGI 3.

**Supplemental Figure S23.** Phenotypes of Tartary buckwheat seedlings infected with *R. solani* AG4-HGI 3 and pretreated with SA, ET, GA, or JA.

**Supplemental Figure S24.** The most significantly enriched GO terms of JA-induced differentially expressed genes in Tartary buckwheat during infection by *R. solani* AG4-HGI 3.

**Supplemental Figure S25.** RT-qPCR analysis of *FtCYP94C1* expression level in leaves of *Arabidopsis* lines heterologously expressing *FtCYP94C1*.

**Supplemental Figure S26.** Relative pathogen biomass of *R. solani* AG4-HGI 3 infected *FtCYP94C1* overexpression lines.

**Supplemental Figure S27.** DAB staining of *Arabidopsis* lines heterologously expressing *FtCYP94C1* and infected by *R. solani* AG4-HGI 3.

**Supplemental Figure S28.** Phenotypes observed on Tartary buckwheat leaves transiently overexpressing *FtCYP94C1* and infected by *R. solani* AG4-HGI 3.

**Supplemental Figure S29.** Phenotype of JA mutants (*aoc4*, *jar1*, and *myc2 myc3 myc4*) and wild-type (Col-0) plants inoculated with *R. solani* AG4-HGI 3 with or without pretreatment with JA.

**Supplemental Figure S30.** Disease resistance of JA mutants (*aoc4*, *jar1*, and *myc2 myc3 myc4*) and wild-type (Col-0) plants infected with *R. solani* AG4-HGI 3 with or without pretreatment with JA.

**Supplemental Figure S31.** Relative pathogen biomass in JA mutants (*aoc4*, *jar1*, and *myc2 myc3 myc4*) and wild-type (Col-0) plants inoculated with *R. solani* AG4-HGI 3 with or without pretreatment with JA.

**Supplemental Figure S32.** PCA for the metabolome data of *Arabidopsis* lines heterologously expressing *FtCYP94C1*. Wild-type (Col-0) plants were used as negative control.

**Supplemental Figure S33.** Flavonoid contents of JA mutants (*aoc4*, *jar1*, and *myc2 myc3 myc4*) and wild-type (Col-0) plants with or without pretreatment with JA.

**Supplemental Figure S34.** Quantile–quantile (Q–Q) plots of the disease index based on the EMMAx algorithm.

**Supplemental Figure S35.** The most significantly enriched KEGG metabolic pathways of GWAS-identified genes in Tartary buckwheat during *R. solani* infection.

**Supplemental Figure S36.** Overlapping GWAS signals between the disease index and the content of disease resistance-associated metabolites (tangertin, indole, and indole-3-carboxylic acid).

**Supplemental Figure S37.** RT-qPCR analysis of *FtASP* expression levels in leaves of *Arabidopsis* lines heterologously expressing *FtASP*.

**Supplemental Figure S38.** Phenotype of *Arabidopsis* lines heterologously expressing the indicated genes identified by GWAS upon infection with *R. solani* AG4-HGI 3.

**Supplemental Figure S39.** Disease resistance of *Arabidopsis* lines heterologously expressing the indicated genes identified by GWAS upon infection with *R. solani* AG4-HGI 3.

**Supplemental Figure S40.** Geographical distribution of Tartary buckwheat accessions.

**Supplemental Figure S41.** Relative pathogen biomass of *Arabidopsis* lines heterologously expressing *FtASP* and infected with *R. solani* AG4-HGI 3.

**Supplemental Figure S42.** DAB staining and MDA content of *Arabidopsis* lines heterologously expressing *FtASP1* infected with *R. solani* AG4-HGI 3.

**Supplemental Figure S43.** Phenotypes observed on Tartary buckwheat leaves transiently overexpressing *FtASP* infected with *R. solani* AG4-HGI 3.

**Supplemental Figure S44.** Immunoblotting with anti-His antibody to detect purified recombinant His-*FtASP* (1 to 225), His-*FtASP*-N (1 to 112), and His-*FtASP*-C (113 to 225).

**Supplemental Figure S45.** Biomass of *R. solani* AG4-HGI 3 grown for 24 h in PDB medium containing purified recombinant His-*FtASP* (1 to 225), His-*FtASP*-N (1 to 112), or His-*FtASP*-C (113 to 225).

**Supplemental Figure S46.** Protease activity assay of *FtASP*.

**Supplemental Data Set 1.** Summary of sequencing data of the *R. solani* AG4-HGI 3 assembly.

**Supplemental Data Set 2.** Genome survey data statistics with *k*-mer frequency distribution.

**Supplemental Data Set 3.** Description of the *R. solani* genome assembly.

**Supplemental Data Set 4.** Evaluation of *R. solani* AG4-HGI 3 sequencing results.

**Supplemental Data Set 5.** Summary of repeat elements in the *R. solani* AG4-HGI 3 assembly.

**Supplemental Data Set 6.** Summary of repeat elements in the genomes of 23 *R. solani* isolates and *M. oryzae*.

**Supplemental Data Set 7.** Orthologous gene families among 23 *R. solani* isolates and *M. oryzae*.

**Supplemental Data Set 8.** Number of gene families, specific family, genes in the family, and unique genes of 23 *R. solani* isolates and *M. oryzae*.

**Supplemental Data Set 9.** List of expanded and contracted gene families in *R. solani* AG4-HGI 3.

**Supplemental Data Set 10.** Analysis of CAZymes in *R. solani* AG4-HGI 3.

**Supplemental Data Set 11.** Characterization of CAZymes in *R. solani*.

**Supplemental Data Set 12.** Characterization of CAZymes involved in lignin, cellulose, hemicellulose, and pectin degradation in *R. solani*.

**Supplemental Data Set 13.** Genes encoding predicted secreted proteins in *R. solani* AG4-HGI 3.

**Supplemental Data Set 14.** Predicted number of secreted proteins of *R. solani*.

**Supplemental Data Set 15.** Genes encoding predicted effector proteins in *R. solani* AG4-HGI 3.

**Supplemental Data Set 16.** Number of predicted effector proteins in *R. solani*.

**Supplemental Data Set 17.** Predicted virulence genes in *R. solani* AG4-HGI 3.

**Supplemental Data Set 18.** Genes encoding predicted interaction proteins between pathogens and plant hosts in *R. solani* AG4-HGI 3.

**Supplemental Data Set 19.** Genes encoding predicted transporters in *R. solani* AG4-HGI 3.

**Supplemental Data Set 20.** Genes encoding predicted transmembrane proteins in *R. solani* AG4-HGI 3.

**Supplemental Data Set 21.** Predicted secondary metabolite biosynthesis gene clusters in *R. solani* AG4-HGI 3.

**Supplemental Data Set 22.** Summary of RNA-seq results in *R. solani* AG4-HGI 3 after infection of Tartary buckwheat.

**Supplemental Data Set 23.** Upregulated genes in *R. solani* AG4-HGI 3 during the *R. solani*–Tartary buckwheat interaction.

**Supplemental Data Set 24.** Gene number with different expression patterns in expanded gene families.

**Supplemental Data Set 25.** Summary of the expression pattern of expanded gene families.

**Supplemental Data Set 26.** Upregulated expanded gene families in *R. solani* AG4-HGI 3 during the *R. solani*–Tartary buckwheat interaction.

**Supplemental Data Set 27.** Downregulated expanded gene families in *R. solani* AG4-HGI 3 during the *R. solani*–Tartary buckwheat interaction.

**Supplemental Data Set 28.** Number of genes with different expression patterns in contracted gene families.

**Supplemental Data Set 29.** Summary of expression patterns of contracted gene families.

**Supplemental Data Set 30.** Upregulated contracted gene families in *R. solani* AG4-HGI 3 during the *R. solani*–Tartary buckwheat interaction.

**Supplemental Data Set 31.** Downregulated contracted gene families in *R. solani* AG4-HGI 3 during the *R. solani*–Tartary buckwheat interaction.

**Supplemental Data Set 32.** Upregulated genes encoding CAZymes in *R. solani* AG4-HGI 3 during *R. solani*–Tartary buckwheat interaction.

**Supplemental Data Set 33.** Number of upregulated genes encoding CAZymes in *R. solani* AG4-HGI 3 during infection of Tartary buckwheat.

**Supplemental Data Set 34.** Number of upregulated genes encoding CAZymes involved in lignin, cellulose, hemicellulose, and pectin degradation in *R. solani* AG4-HGI 3 during infection of Tartary buckwheat.

**Supplemental Data Set 35.** Candidate interaction proteins of RsYTHDC in Tartary buckwheat identified by combination of pull down and mass spectrometry.

**Supplemental Data Set 36.** Candidate interaction proteins of RsDAD in Tartary buckwheat identified by combination of pull down and mass spectrometry.

**Supplemental Data Set 37.** Summary of RNA-seq results in Tartary buckwheat after infection by *R. solani* AG4-HGI 3.

**Supplemental Data Set 38.** Differentially expressed genes in Tartary buckwheat during the *R. solani*–Tartary buckwheat interaction.

**Supplemental Data Set 39.** Differentially expressed JA biosynthesis and signaling genes in Tartary buckwheat during the *R. solani*–Tartary buckwheat interaction.

**Supplemental Data Set 40.** Summary of RNA-seq results in Tartary buckwheat after treatment with MeJA.

**Supplemental Data Set 41.** Differentially expressed Tartary buckwheat genes shared during the *R. solani*–Tartary buckwheat interaction and following MeJA treatment.

**Supplemental Data Set 42.** Metabolites with different abundance between *FtCYP4502* overexpression lines and wild type.

**Supplemental Data Set 43.** Disease index of the 320 Tartary buckwheat accessions used in this study.

**Supplemental Data Set 44.** Candidate genes associated with disease resistance identified by GWAS.

**Supplemental Data Set 45.** Overlapping GWAS regions between disease resistance and disease resistance–associated metabolite content.

**Supplemental Data Set 46.** Candidate genes identified by GWAS with different expression levels during the *R. solani*–Tartary buckwheat interaction and following JA treatment.



**Supplemental Data Set 47.** Primers used in this study.

**Supplemental Data Set 48.** Summary of statistical analyses.

**Supplemental File 1.** Multiple sequence alignment for the phylogenetic tree shown in Fig. 1A.

**Supplemental File 2.** Tree file for the phylogenetic tree shown in Fig. 1A.

**Supplemental File 3.** Multiple sequence alignment for the phylogenetic tree shown in Fig. 4A.

**Supplemental File 4.** Tree file for the phylogenetic tree shown in Fig. 4A.

**Supplemental File 5.** Multiple sequence alignment for the phylogenetic tree shown in Fig. 6C.

**Supplemental File 6.** Tree file for the phylogenetic tree shown in Fig. 6C.

*Conflict of interest statement.* None declared.

## Funding

This research was supported by National Natural Science Foundation of China (32161143005, 31901511, 31871536 and 31801427), the Project of Sanya Yazhou Bay Science and Technology City (SCKJ-JYRC-2022-22), the Youth Innovation Program of Chinese Academy of Agricultural Sciences (Y2022QC02), National Key R&D Program of China (2017YFE0117600, 2019YFD1000700/2019YFD1000701), European Union Horizon 2020 project Planta SYST (SGA-CSA No. 739582 under FPA No.664620) and China National Postdoctoral Program for Innovative Talents (BX20200377).

## References

- Almagro Armenteros JJ, Tsirigos KD, Sønderby CK, Petersen TN, Winther O, Brunak S, von Heijne G, Nielsen H.** SignalP 5.0 improves signal peptide predictions using deep neural networks. *Nat Biotechnol.* 2019;**37**(4):420–423. <https://doi.org/10.1038/s41587-019-0036-z>
- Anderson JP, Sperschneider J, Win J, Kidd B, Yoshida K, Hane J, Saunders DGO, Singh KB.** Comparative secretome analysis of *Rhizoctonia solani* isolates with different host ranges reveals unique secretomes and cell death inducing effectors. *Sci Rep.* 2017;**7**(1):10410. <https://doi.org/10.1038/s41598-017-10405-y>
- Ao Y, Li Z, Feng D, Xiong F, Liu J, Li JF, Wang M, Wang J, Liu B, Wang HB.** OsCERK1 and OsRLCK176 play important roles in peptidoglycan and chitin signaling in rice innate immunity. *Plant J.* 2014;**80**(6):1072–1084. <https://doi.org/10.1111/tpj.12710>
- Bach-Pages M, Preston GM.** Methods to quantify biotic-induced stress in plants. *Methods Mol Biol.* 2018;**1734**:241–255. [https://doi.org/10.1007/978-1-4939-7604-1\\_19](https://doi.org/10.1007/978-1-4939-7604-1_19)
- Bai X, Zhan G, Tian S, Peng H, Cui X, Islam MA, Goher F, Ma Y, Kang Z, Xu ZS, et al.** Transcription factor BZR2 activates chitinase *Cht20.2* transcription to confer resistance to wheat stripe rust. *Plant Physiol.* 2021;**187**(4):2749–2762. <https://doi.org/10.1093/plphys/kiab383>
- Bari R, Jones JD.** Role of plant hormones in plant defence responses. *Plant Mol Biol.* 2009;**69**(4):473–488. <https://doi.org/10.1007/s11103-008-9435-0>
- Bienert MD, Siegmund SE, Drozak A, Trombik T, Bultreys A, Baldwin IT, Boutry M.** A pleiotropic drug resistance transporter in *Nicotiana tabacum* is involved in defense against the herbivore *Manduca sexta*. *Plant J.* 2012;**72**(5):745–757. <https://doi.org/10.1111/j.1365-313X.2012.05108.x>
- Borras-Hidalgo O, Caprari C, Hernandez-Estevéz I, Lorenzo GD, Cervone F.** A gene for plant protection: expression of a bean polygalacturonase inhibitor in tobacco confers a strong resistance against *Rhizoctonia solani* and two oomycetes. *Front Plant Sci.* 2012;**3**:268. <https://doi.org/10.3389/fpls.2012.00268>
- Brymora A, Valova VA, Robinson PJ.** Protein–protein interactions identified by pull-down experiments and mass spectrometry. *Curr Protoc Cell Biol.* 2004;Capter **17**:Unit 17.5. <https://doi.org/10.1002/0471143030.cb1705s22>
- Buchfink B, Xie C, Huson DH.** Fast and sensitive protein alignment using DIAMOND. *Nat Methods.* 2015;**12**(1):59–60. <https://doi.org/10.1038/nmeth.3176>
- Bundó M, Coca M.** Enhancing blast disease resistance by overexpression of the calcium-dependent protein kinase *OsCPK4* in rice. *Plant Biotechnol J.* 2016;**14**(6):1357–1367. <https://doi.org/10.1111/pbi.12500>
- Bundó M, Coca M.** Calcium-dependent protein kinase *OsCPK10* mediates both drought tolerance and blast disease resistance in rice plants. *J Exp Bot.* 2017;**68**(11):2963–2975. <https://doi.org/10.1093/jxb/erx145>
- Cantarel BL, Coutinho PM, Rancurel C, Bernard T, Lombard V, Henrissat B.** The carbohydrate-active enzymes database (CAZY): an expert resource for glycogenomics. *Nucleic Acids Res.* 2009;**37**-(Database issue):D233–D238. <https://doi.org/10.1093/nar/gkn663>
- Cantarel BL, Korf I, Robb SM, Parra G, Ross E, Moore B, Holt C, Sánchez Alvarado A, Yandell M.** MAKER: an easy-to-use annotation pipeline designed for emerging model organism genomes. *Genome Res.* 2008;**18**(1):188–196. <https://doi.org/10.1101/gr.6743907>
- Chen H, Li C, Liu L, Zhao J, Cheng X, Jiang G, Zhai W.** The Fd-GOGAT1 mutant gene *lc7* confers resistance to *Xanthomonas oryzae* pv. *Oryzae* in rice. *Sci Rep.* 2016;**6**(1):26411. <https://doi.org/10.1038/srep26411>
- Chen C, Zhang K, Khurshid M, Li J, He Ming, Georgiev MI, Zhang X, Zhou M.** MYB Transcription repressors regulate plant secondary metabolism. *Crit Rev Plant Sci.* 2019;**38**(3):159–170. <https://doi.org/10.1080/07352689.2019.1632542>
- Chen S, Zhou Y, Chen Y, Gu J.** Fastp: an ultra-fast all-in-one FASTQ preprocessor. *Bioinformatics* 2018;**34**(17):i884–i890. <https://doi.org/10.1093/bioinformatics/bty560>
- Choe S, Choi B, Kang JH, Seo JK.** Tolerance to tomato yellow leaf curl virus in transgenic tomato overexpressing a cellulose synthase-like gene. *Plant Biotechnol J.* 2021;**19**(4):657–659. <https://doi.org/10.1111/pbi.13539>
- Clough SJ, Bent AF.** Floral dip: a simplified method for *Agrobacterium*-mediated transformation of *Arabidopsis thaliana*. *Plant J.* 1998;**16**(6):735–743. <https://doi.org/10.1046/j.1365-313x.1998.00343.x>
- Cui W, Wang S, Han K, Zheng E, Ji M, Chen B, Wang X, Chen J, Yan F.** Ferredoxin 1 is downregulated by the accumulation of abscisic acid in an ABI5-dependent manner to facilitate rice stripe virus infection in *Nicotiana benthamiana* and rice. *Plant J.* 2021;**107**(4):1183–1197. <https://doi.org/10.1111/tpj.15377>
- Dean R, Van Kan JAV, Pretorius ZA, Hammond-Kosack KE, Pietro AD, Spanu PD, Rudd JJ, Dickman M, Kahmann R, Ellis J, et al.** The top 10 fungal pathogens in molecular plant pathology. *Mol Plant Pathol.* 2012;**13**(4):414–430. <https://doi.org/10.1111/j.1364-3703.2011.00783.x>
- De Geyter N, Gholami A, Goormachtig S, Goossens A.** Transcriptional machineries in jasmonate-elicited plant secondary metabolism. *Trends Plant Sci.* 2012;**17**(6):349–359. <https://doi.org/10.1016/j.tplants.2012.03.001>
- Ding M, Zhang K, He Y, Zuo Q, Zhao H, He M, Georgiev MI, Park SU, Zhou M.** FtBPM3 modulates the orchestration of FtMYB11-mediated flavonoids biosynthesis in Tartary buckwheat. *Plant Biotechnol J.* 2021;**19**(7):1285–1287. <https://doi.org/10.1111/pbi.13587>

- Dong Z, Li W, Liu J, Li L, Pan S, Liu S, Gao J, Liu L, Liu X, Wang GL, et al.** The rice phosphate transporter protein OsPT8 regulates disease resistance and plant growth. *Sci Rep.* 2019;**9**(1):5408. <https://doi.org/10.1038/s41598-019-41718-9>
- Dong C, Li R, Wang N, Liu Y, Zhang Y, Bai S.** Apple vacuolar processing enzyme 4 modulates fruit disease resistance and is regulated by cysteine protease inhibitor. *J Exp Bot.* 2022;**73**(11):3758–3773. <https://doi.org/10.1093/jxb/erac093>
- Duan H, Jones AW, Hewitt T, Mackenzie A, Hu Y, Sharp A, Lewis D, Mago R, Upadhyaya NM, Rathjen JP, et al.** Physical separation of haplotypes in dikaryons allows benchmarking of phasing accuracy in Nanopore and HiFi assemblies with Hi-C data. *Genome Biol.* 2022;**23**(1):84. <https://doi.org/10.1186/s13059-022-02658-2>
- Eddy SR.** Profile hidden Markov models. *Bioinformatics* 1998;**14**(9):755–763. <https://doi.org/10.1093/bioinformatics/14.9.755>
- Edgar RC.** MUSCLE: multiple sequence alignment with high accuracy and high throughput. *Nucleic Acids Res.* 2004;**32**(5):1792–1797. <https://doi.org/10.1093/nar/gkh340>
- Feng H, Wang X, Zhang Q, Fu Y, Feng C, Wang B, Huang L, Kang Z.** Monodehydroascorbate reductase gene, regulated by the wheat PN-2013 miRNA, contributes to adult wheat plant resistance to stripe rust through ROS metabolism. *Biochim Biophys Acta.* 2014;**1839**(1):1–12. <https://doi.org/10.1016/j.bbagr.2013.11.001>
- Fernández-Calvo P, Chini A, Fernández-Barbero G, Chico J-M, Gimenez-Ibanez S, Geerinck J, Eeckhout D, Schweizer F, Godoy M, Franco-Zorrilla JM, et al.** The *Arabidopsis* bHLH transcription factors MYC3 and MYC4 are targets of JAZ repressors and act additively with MYC2 in the activation of jasmonate responses. *Plant Cell.* 2011;**23**(2):701–715. <https://doi.org/10.1105/tpc.110.080788>
- Ferrari S, Vairo D, Ausubel FM, Cervone F, De Lorenzo G.** Tandemly duplicated *Arabidopsis* genes that encode polygalacturonase-inhibiting proteins are regulated coordinately by different signal transduction pathways in response to fungal infection. *Plant Cell* 2003;**15**(1):93–106. <https://doi.org/10.1105/tpc.005165>
- Gamir J, Pastor V, Cerezo M, Flors V.** Identification of indole-3-carboxylic acid as mediator of priming against *Plectosphaerella cucumerina*. *Plant Physiol Biochem.* 2012;**61**:169–179. <https://doi.org/10.1016/j.plaphy.2012.10.004>
- Ger MJ, Louh GY, Lin YH, Feng TY, Huang HE.** Ectopically expressed sweet pepper ferredoxin PFLP enhances disease resistance to *Pectobacterium carotovorum* subsp. *carotovorum* affected by harpin and protease-mediated hypersensitive response in *Arabidopsis*. *Mol Plant Pathol.* 2014;**15**(9):892–906. <https://doi.org/10.1111/mpp.12150>
- Hane JK, Anderson JP, Williams AH, Sperschnieder J, Singh KB.** Genome sequencing and comparative genomics of the broad host-range pathogen *Rhizoctonia solani* AG8. *PLoS Genet.* 2014;**10**(5):e1004281. <https://doi.org/10.1371/journal.pgen.1004281>
- He M, He Y, Zhang K, Lu X, Zhang X, Gao B, Fan Y, Zhao H, Jha R, Huda MN, et al.** Comparison of buckwheat genomes reveals the genetic basis of metabolomic divergence and ecotype differentiation. *New Phytologist.* 2022;**235**(5):1927–1943. <https://doi.org/10.1111/nph.18306>
- He Y, Wu L, Liu X, Jiang P, Yu L, Qiu J, Wang G, Zhang X, Ma H.** *TaUGT6*, a novel UDP-glycosyltransferase gene enhances the resistance to FHB and DON accumulation in wheat. *Front Plant Sci.* 2020;**11**:574775. <https://doi.org/10.3389/fpls.2020.574775>
- Heitz T, Widemann E, Lugan R, Miesch L, Ullmann P, Désaubry L, Holder E, Grausem B, Kandel S, Miesch M, et al.** Cytochromes P450 CYP94C1 and CYP94B3 catalyze two successive oxidation steps of plant hormone jasmonoyl-isoleucine for catabolic turnover. *J Biol Chem.* 2012;**287**(9):6296–6306. <https://doi.org/10.1074/jbc.M111.316364>
- Hernández-Blanco C, Feng DX, Hu J, Sánchez-Vallet A, Deslandes L, Llorente F, Berrocal-Lobo M, Keller H, Barlet X, Sánchez-Rodríguez C, et al.** Impairment of cellulose synthases required for *Arabidopsis* secondary cell wall formation enhances disease resistance. *Plant Cell* 2007;**19**(3):890–903. <https://doi.org/10.1105/tpc.106.048058>
- Hu P, Meng Y, Wise RP.** Functional contribution of chorismate synthase, anthranilate synthase, and chorismate mutase to penetration resistance in barley-powdery mildew interactions. *Mol Plant Microbe Interact.* 2009;**22**(3):311–320. <https://doi.org/10.1094/MPMI-22-3-0311>
- Huang HE, Ger MJ, Chen CY, Pandey AK, Yip MK, Chou HW, Feng TY.** Disease resistance to bacterial pathogens affected by the amount of ferredoxin-I protein in plants. *Mol Plant Pathol.* 2007;**8**(1):129–137. <https://doi.org/10.1111/j.1364-3703.2006.00378.x>
- Jones P, Binns D, Chang H-Y, Fraser M, Li W, McAnulla C, McWilliam H, Maslen J, Mitchell A, Nuka G, et al.** Interproscan 5: genome-scale protein function classification. *Bioinformatics* 2014;**30**(9):1236–1240. <https://doi.org/10.1093/bioinformatics/btu031>
- Kang HM, Sul JH, Service SK, Zaitlen NA, Kong SY, Freimer NB, Sabatti C, Eskin E.** Variance component model to account for sample structure in genome-wide association studies. *Nat Genet.* 2010;**42**(4):348–354. <https://doi.org/10.1038/ng.548>
- Kankanala P, Nandety RS, Mysore KS.** Genomics of plant disease resistance in legumes. *Front Plant Sci.* 2019;**10**:1345. <https://doi.org/10.3389/fpls.2019.01345>
- Karki SJ, Reilly A, Zhou B, Mascarello M, Burke J, Doohan F, Douchkov D, Schweizer P, Feechan A.** A small secreted protein from *Zymoseptoria tritici* interacts with a wheat E3 ubiquitin ligase to promote disease. *J Exp Bot.* 2021;**72**(2):733–746. <https://doi.org/10.1093/jxb/eraa489>
- Kaushik A, Roberts DP, Ramaprasad A, Mfarrej S, Nair M, Lakshman DK, Pain A.** Pangenome analysis of the soilborne fungal phytopathogen *Rhizoctonia solani* and development of a comprehensive web resource: RsolaniDB. *Front Microbiol.* 2022;**13**:839524. <https://doi.org/10.3389/fmicb.2022.839524>
- Khare D, Choi H, Huh SU, Bassin B, Kim J, Martinoia E, Sohn KH, Paek KH, Lee Y.** *Arabidopsis* ABCG34 contributes to defense against necrotrophic pathogens by mediating the secretion of camalexin. *Proc Natl Acad Sci U S A.* 2017;**114**(28):E5712–E5720. <https://doi.org/10.1073/pnas.1702259114>
- Kim D, Langmead B, Salzberg SL.** HISAT: a fast spliced aligner with low memory requirements. *Nat Methods.* 2015;**12**(4):357–360. <https://doi.org/10.1038/nmeth.3317>
- Ko M, Cho JH, Seo HH, Lee HH, Kang HY, Nguyen TS, Soh HC, Kim YS, Kim JI.** Constitutive expression of a fungus-inducible carboxylesterase improves disease resistance in transgenic pepper plants. *Planta* 2016;**244**(2):379–392. <https://doi.org/10.1007/s00425-016-2514-6>
- Koo AJ, Cooke TF, Howe GA.** Cytochrome P450 CYP94B3 mediates catabolism and inactivation of the plant hormone jasmonoyl-L-isoleucine. *Proc Natl Acad Sci U S A.* 2011;**108**(22):9298–9303. <https://doi.org/10.1073/pnas.1103542108>
- Koo AJ, Thireault C, Zemelis S, Poudel AN, Zhang T, Kitaoka N, Brandizzi F, Matsuura H, Howe GA.** Endoplasmic reticulum-associated inactivation of the hormone jasmonoyl-L-isoleucine by multiple members of the cytochrome P450 94 family in *Arabidopsis*. *J Biol Chem.* 2014;**289**(43):29728–29738. <https://doi.org/10.1074/jbc.M114.603084>
- Koren S, Walenz BP, Berlin K, Miller JR, Bergman NH, Phillippy AM.** Canu: scalable and accurate long-read assembly via adaptive k-mer weighting and repeat separation. *Genome Res.* 2017;**27**(5):722–736. <https://doi.org/10.1101/gr.215087.116>
- Kouzai Y, Kimura Mamiko, Watanabe Megumi, Kusunoki Kazuki, Osaka Daiki, Suzuki Tomoko, Matsui Hidenori, Yamamoto Mikihiko, Ichinose Yuki, Toyoda Kazuhiro, et al.** Salicylic acid-dependent immunity contributes to resistance against *Rhizoctonia solani*, a necrotrophic fungal agent of sheath blight, in rice and *Brachypodium distachyon*. *New Phytol.* 2018;**217**(2):771–783. <https://doi.org/10.1111/nph.14849>
- Kumar S, Stecher G, Li M, Knyaz C, Tamura K.** MEGA X: molecular evolutionary genetics analysis across computing platforms. *Mol*

- Biol. Evol. 2018;**35**(6):1547–1549. <https://doi.org/10.1093/molbev/msy096>
- Kurtz S, Phillippy A, Delcher AL, Smoot M, Shumway M, Antonescu C, Salzberg SL.** Versatile and open software for comparing large genomes. *Genome Biol.* 2004;**5**(2):R12. <https://doi.org/10.1186/gb-2004-5-2-r12>
- Lee DY, Jeon J, Kim K-T, Cheong K, Song H, Choi G, Ko J, Opiyo SO, Correll JC, Zuo S, et al.** Comparative genome analyses of four rice-infecting *Rhizoctonia solani* isolates reveal extensive enrichment of homogalacturonan modification genes. *BMC Genomics* 2021;**22**(1):242. <https://doi.org/10.1186/s12864-021-07549-7>
- Li, H.** Aligning sequence reads, clone sequences and assembly contigs with BWA-MEM. arXiv:1303.3997v2. 2013
- Li B, Dewey CN.** RSEM: accurate transcript quantification from RNA-seq data with or without a reference genome. *BMC Bioinformatics* 2011;**12**:323. <https://doi.org/10.1186/1471-2105-12-323>
- Li C, Guo Z, Zhou S, Han Q, Zhang M, Peng Y, Hsiang T, Chen X.** Evolutionary and genomic comparisons of hybrid uninucleate and nonhybrid *Rhizoctonia* fungi. *Commun Biol.* 2021;**4**(1):201. <https://doi.org/10.1038/s42003-021-01724-y>
- Li D, Li S, Wei S, Sun W.** Strategies to manage rice sheath blight: lessons from interactions between rice and *Rhizoctonia solani*. *Rice (N Y).* 2021;**14**(1):21. <https://doi.org/10.1186/s12284-021-00466-z>
- Li N, Lin B, Wang H, Li X, Yang F, Ding X, Yan J, Chu Z.** Natural variation in *ZmFBL41* confers banded leaf and sheath blight resistance in maize. *Nat Genet.* 2019;**51**(10):1540–1548. <https://doi.org/10.1038/s41588-019-0503-y>
- Li L, Stoekert CJ, Roos DS.** OrthoMCL: identification of ortholog groups for eukaryotic genomes. *Genome Res.* 2003;**13**(9):2178–2189. <https://doi.org/10.1101/gr.1224503>
- Li S, Zhang K, Khurshid M, Fan Y, Xu B, Zhou M.** First report of *Rhizoctonia solani* AG-4 HGI causing stem canker on *Fagopyrum tataricum* (Tartary buckwheat) in China. *Plant Dis.* 2021;**105**(2):505. <https://doi.org/10.1094/PDIS-06-20-1253-PDN>
- Liang M, Ye H, Shen Q, Jiang X, Cui G, Gu W, Zhang LH, Naqvi NI, Deng YZ.** Tangeretin inhibits fungal ferroptosis to suppress rice blast. *J Integr Plant Biol.* 2021;**63**(12):2136–2149. <https://doi.org/10.1111/jipb.13175>
- Liu F, Huang N, Wang L, Ling H, Sun T, Ahmad W, Muhammad K, Guo J, Xu L, Gao S, et al.** A novel L-ascorbate peroxidase 6 gene, *ScAPX6*, plays an important role in the regulation of response to biotic and abiotic stresses in sugarcane. *Front Plant Sci.* 2018;**8**:2262. <https://doi.org/10.3389/fpls.2017.02262>
- Liu H, Ma Y, Chen N, Guo S, Liu H, Guo X, Chong K, Xu Y.** Overexpression of stress-inducible OsBURP16, the  $\beta$  subunit of polygalacturonase 1, decreases pectin content and cell adhesion and increases abiotic stress sensitivity in rice. *Plant Cell Environ.* 2014;**37**(5):1144–1158. <https://doi.org/10.1111/pce.12223>
- Liu S, Zhang X, Xiao S, Ma J, Shi W, Qin T, Xi H, Nie X, You C, Xu Z, et al.** A single-nucleotide mutation in a GLUTAMATE RECEPTOR-LIKE gene confers resistance to Fusarium wilt in *Gossypium hirsutum*. *Adv Sci.* 2021;**8**(7):2002723. <https://doi.org/10.1002/advs.202002723>
- Love MI, Huber W, Anders S.** Moderated estimation of fold change and dispersion for RNA-seq data with DESeq2. *Genome Biol.* 2014;**15**(12):550. <https://doi.org/10.1186/s13059-014-0550-8>
- Lowie TM, Eddy SR.** tRNAscan-SE: a program for improved detection of transfer RNA genes in genomic sequence. *Nucleic Acids Res.* 1997;**25**(5):955–964. <https://doi.org/10.1093/nar/25.5.955>
- Lu YJ, Li P, Shimono M, Corrion A, Higaki T, He SY, Day B.** *Arabidopsis* calcium-dependent protein kinase 3 regulates actin cytoskeleton organization and immunity. *Nat Commun.* 2020;**11**(1):6234. <https://doi.org/10.1038/s41467-020-20007-4>
- Mat Razali N, Hisham SN, Kumar IS, Shukla RN, Lee M, Abu Bakar MF, Nadarajah K.** Comparative genomics: insights on the pathogenicity and lifestyle of *Rhizoctonia solani*. *Int J Mol Sci.* 2021;**22**(4):2183. <https://doi.org/10.3390/ijms22042183>
- McKenna A, Hanna M, Banks E, Sivachenko A, Cibulskis K, Kernytsky A, Garimella K, Altshuler D, Gabriel S, Daly M, et al.** The genome analysis toolkit: a MapReduce framework for analyzing next-generation DNA sequencing data. *Genome Res.* 2010;**20**(9):1297–1303. <https://doi.org/10.1101/gr.107524.110>
- Mhamdi A, Mauve C, Gouia H, Saindrenan P, Hodges M, Noctor G.** Cytosolic NADP-dependent isocitrate dehydrogenase contributes to redox homeostasis and the regulation of pathogen responses in *Arabidopsis* leaves. *Plant Cell Environ.* 2010;**33**(7):1112–1123. <https://doi.org/10.1111/j.1365-3040.2010.02133.x>
- Misra P, Pandey A, Tiwari M, Chandrashekar K, Sidhu OP, Asif MH, Chakrabarty D, Singh PK, Trivedi PK, Nath P, et al.** Modulation of transcriptome and metabolome of tobacco by *Arabidopsis* transcription factor, *AtMYB12*, leads to insect resistance. *Plant Physiol.* 2010;**152**(4):2258–2268. <https://doi.org/10.1104/pp.109.150979>
- Moeder W, Urquhart W, Ung H, Yoshioka K.** The role of cyclic nucleotide-gated ion channels in plant immunity. *Mol Plant.* 2011;**4**(3):442–452. <https://doi.org/10.1093/mp/ssr018>
- Molla KA, Karmakar S, Molla J, Bajaj P, Varshney RK, Datta SK, Datta K.** Understanding sheath blight resistance in rice: the road behind and the road ahead. *Plant Biotechnol J.* 2020;**18**(4):895–915. <https://doi.org/10.1111/pbi.13312>
- Moreno JI, Martín R, Castresana C.** *Arabidopsis* SHMT1, a serine hydroxymethyltransferase that functions in the photorespiratory pathway influences resistance to biotic and abiotic stress. *Plant J.* 2005;**41**(3):451–463. <https://doi.org/10.1111/j.1365-313X.2004.02311.x>
- Mutuku JM, Nose A.** Changes in the contents of metabolites and enzyme activities in rice plants responding to *Rhizoctonia solani* Kuhn infection: activation of glycolysis and connection to phenylpropanoid pathway. *Plant Cell Physiol.* 2012;**53**(6):1017–1032. <https://doi.org/10.1093/pcp/pcs047>
- Oh SK, Baek KH, Seong ES, Joung YH, Choi GJ, Park JM, Cho HS, Kim EA, Lee S, Choi D.** CamSRB2, pepper methionine sulfoxide reductase B2, is a novel defense regulator against oxidative stress and pathogen attack. *Plant Physiol.* 2010;**154**(1):245–261. <https://doi.org/10.1104/pp.110.162339>
- Pan L, Zhao X, Chen M, Fu Y, Xiang M, Chen J.** Effect of exogenous methyl jasmonate treatment on disease resistance of postharvest kiwifruit. *Food Chem.* 2020;**305**:125483. <https://doi.org/10.1016/j.foodchem.2019.125483>
- Pandey SP, Somssich IE.** The role of WRKY transcription factors in plant immunity. *Plant Physiol.* 2009;**150**(4):1648–1655. <https://doi.org/10.1104/pp.109.138990>
- Paparella C, Savatin DV, Marti L, De Lorenzo G, Ferrari S.** The *Arabidopsis* LYSIN MOTIF-CONTAINING RECEPTOR-LIKE KINASE3 regulates the cross talk between immunity and abscisic acid responses. *Plant Physiol.* 2014;**165**(1):262–276. <https://doi.org/10.1104/pp.113.233759>
- Park DS, Saylor RJ, Hong YG, Nam MH, Yang Y.** A method for inoculation and evaluation of rice sheath blight disease. *Plant Dis.* 2008;**92**(1):25–29. <https://doi.org/10.1094/PDIS-92-1-0025>
- Pasquet JC, Changenet V, Macadré C, Boex-Fontvieille E, Soulhat C, Bouchabké-Coussa O, Dalmais M, Atanasova-Pénichon V, Bendahmane A, Saindrenan P, et al.** A *Brachypodium* UDP-glycosyltransferase confers root tolerance to deoxynivalenol and resistance to *Fusarium* infection. *Plant Physiol.* 2016;**172**(1):559–574. <https://doi.org/10.1104/pp.16.00371>
- Pastor-Fernández J, Pastor V, Mateu D, Gamir J, Sánchez-Bel P, Flors V.** Accumulating evidences of callose priming by indole-3-carboxylic acid in response to *Plectosphaera cucumerina*. *Plant Signal Behav.* 2019;**14**(7):1608107. <https://doi.org/10.1080/15592324.2019.1608107>
- Peng C, Liang X, Liu EE, Zhang JJ, Peng XX.** The oxalyl-CoA synthetase-regulated oxalate and its distinct effects on resistance to bacterial blight and aluminium toxicity in rice. *Plant Biol (Stuttg).* 2017;**19**(3):345–353. <https://doi.org/10.1111/plb.12542>



- Pertea M, Pertea GM, Antonescu CM, Chang TC, Mendell JT, Salzberg SL.** Stringtie enables improved reconstruction of a transcriptome from RNA-seq reads. *Nat Biotechnol.* 2015;**33**(3): 290–295. <https://doi.org/10.1038/nbt.3122>
- Poudel AN, Holtsclaw RE, Kimberlin A, Sen S, Zeng S, Joshi T, Lei Z, Sumner LW, Singh K, Matsuura H, et al.** 12-Hydroxy-jasmonoyl-L-isoleucine is an active jasmonate that signals through CORONATINE INSENSITIVE 1 and contributes to the wound response in *Arabidopsis*. *Plant Cell Physiol.* 2019;**60**(10):2152–2166. <https://doi.org/10.1093/pcp/pcz109>
- Prasad BD, Creissen G, Lamb C, Chattoo BB.** Overexpression of rice (*Oryza sativa* L.) *OsCDR1* leads to constitutive activation of defense responses in rice and *Arabidopsis*. *Mol Plant Microbe Interact.* 2009;**22**(12):1635–1644. <https://doi.org/10.1094/MPMI-22-12-1635>
- Qin X, Pi X, Wang W, Han G, Zhu L, Liu M, Cheng L, Shen J, Kuang T, Sui S.** Structure of a green algal photosystem I in complex with a large number of light-harvesting complex I subunits. *Nat Plants.* 2019;**5**(3): 263–272. <https://doi.org/10.1038/s41477-019-0379-y>
- Rhie A, Walenz BP, Koren S, Phillippy AM.** Merqury: reference-free quality, completeness, and phasing assessment for genome assemblies. *Genome Biol.* 2020;**21**(1):245. <https://doi.org/10.1186/s13059-020-02134-9>
- Robinson MD, McCarthy DJ, Smyth GK.** Edger: a Bioconductor package for differential expression analysis of digital gene expression data. *Bioinformatics* 2010;**26**(1):139–140. <https://doi.org/10.1093/bioinformatics/btp616>
- Saitou N, Nei M.** The neighbor-joining method: a new method for reconstructing phylogenetic trees. *Mol Biol Evol.* 1987;**4**(4):406–425. <https://doi.org/10.1093/oxfordjournals.molbev.a040454>
- Sasse J, Schlegel M, Borghi L, Ullrich F, Lee M, Liu GW, Giner JL, Kayser O, Bigler L, Martinoia E, et al.** *Petunia hybrida* PDR2 is involved in herbivore defense by controlling steroidal contents in trichomes. *Plant Cell Environ.* 2016;**39**(12):2725–2739. <https://doi.org/10.1111/pce.12828>
- Schenke D, Utami HP, Zhou Z, Gallegos MT, Cai D.** Suppression of UV-B stress induced flavonoids by biotic stress: is there reciprocal crosstalk? *Plant Physiol Biochem.* 2019;**134**:53–63. <https://doi.org/10.1016/j.plaphy.2018.06.026>
- Seemann T.** Prokka: rapid prokaryotic genome annotation. *Bioinformatics* 2014;**30**(14):2068–2069. <https://doi.org/10.1093/bioinformatics/btu153>
- Shen Q, Liu L, Wang L, Wang Q.** Indole primes plant defense against necrotrophic fungal pathogen infection. *PLoS One* 2018;**13**(11): e0207607. <https://doi.org/10.1371/journal.pone.0207607>
- Shi H, Liu W, Yao Y, Wei Y, Chan Z.** *Alcohol dehydrogenase 1 (ADH1)* confers both abiotic and biotic stress resistance in *Arabidopsis*. *Plant Sci.* 2017;**262**:24–31. <https://doi.org/10.1016/j.plantsci.2017.05.013>
- Shu X, Wang A, Jiang B, Jiang Y, Xiang X, Yi X, Li S, Deng Q, Wang S, Zhu J, et al.** Genome-wide association study and transcriptome analysis discover new genes for bacterial leaf blight resistance in rice (*Oryza sativa* L.). *BMC Plant Biol.* 2021;**21**(1):255. <https://doi.org/10.1186/s12870-021-03041-2>
- Sperschneider J, Dodds PN.** EffectorP 3.0: prediction of apoplastic and cytoplasmic effectors in fungi and oomycetes. *Mol Plant Microbe Interact.* 2022;**35**(2):146–156. <https://doi.org/10.1094/MPMI-08-21-0201-R>
- Stamatakis A.** RAxML version 8: a tool for phylogenetic analysis and post-analysis of large phylogenies. *Bioinformatics* 2014;**30**(9): 1312–1213. <https://doi.org/10.1093/bioinformatics/btu033>
- Taheri P, Tarighi S.** Riboflavin induces resistance in rice against *Rhizoctonia solani* via jasmonate-mediated priming of phenylpropanoid pathway. *J Plant Physiol.* 2010;**167**(3):201–208. <https://doi.org/10.1016/j.jplph.2009.08.003>
- Takahashi M, Sriswasdi S, Manabe RI, Ohkuma M, Sugita T, Iwasaki W.** A Trichosporonales genome tree based on 27 haploid and three evolutionarily conserved ‘natural’ hybrid genomes. *Yeast* 2018;**35**(1): 99–111. <https://doi.org/10.1002/yea.3284>
- Tarailo-Graovac M, Chen N.** Using RepeatMasker to identify repetitive elements in genomic sequences. *Curr Protoc Bioinformatics Chapter.* 2009;Chapter 4:4.10.1–4.10.14. <https://doi.org/10.1002/0471250953.bi0410s25>
- Tian S, Wang X, Li P, Wang H, Ji H, Xie J, Qiu Q, Shen D, Dong H.** Plant aquaporin AtPIP1; 4 links apoplastic H<sub>2</sub>O<sub>2</sub> induction to disease immunity pathways. *Plant Physiol.* 2016;**171**(3):1635–1650. <https://doi.org/10.1104/pp.15.01237>
- Ullah C, Unsicker SB, Fellenberg C, Constabel CP, Schmidt A, Gershenzon J, Hammerbacher A.** Flavan-3-ols are an effective chemical defense against rust infection. *Plant Physiol.* 2017;**175**(4): 1560–1578. <https://doi.org/10.1104/pp.17.00842>
- Vaser R, Sović I, Nagarajan N, Šikić M.** Fast and accurate de novo genome assembly from long uncorrected reads. *Genome Res.* 2017;**27**(5): 737–746. <https://doi.org/10.1101/gr.214270.116>
- Verma V, Ravindran P, Kumar PP.** Plant hormone-mediated regulation of stress responses. *BMC Plant Biol.* 2016;**16**(1):86. <https://doi.org/10.1186/s12870-016-0771-y>
- Vurture GW, Sedlazeck FJ, Nattestad M, Underwood CJ, Fang H, Gurtowski J, Schatz MC.** GenomeScope: fast reference-free genome profiling from short reads. *Bioinformatics.* 2017;**33**(14):2202–2204. <http://dx.doi.org/10.1093/bioinformatics/btx153>
- Waghu FH, Idicula-Thomas S.** Collection of antimicrobial peptides database and its derivatives: applications and beyond. *Protein Sci.* 2020;**29**(1):36–42. <https://doi.org/10.1002/pro.3714>
- Wallon T, Sauvageau A, Heyden HV.** Detection and quantification of *Rhizoctonia solani* and *Rhizoctonia solani* AG1-IB causing the bottom rot of lettuce in tissues and soils by multiplex qPCR. *Plants (Basel)* 2020;**10**(1):57. <https://doi.org/10.3390/plants10010057>
- Wally O, Punja ZK.** Enhanced disease resistance in transgenic carrot (*Daucus carota* L.) plants over-expressing a rice cationic peroxidase. *Planta* 2010;**232**(5):1229–1239. <https://doi.org/10.1007/s00425-010-1252-4>
- Wan J, Tanaka K, Zhang XC, Son GH, Brechenmacher L, Nguyen TH, Stacey G.** LYK4, a lysin motif receptor-like kinase, is important for chitin signaling and plant innate immunity in *Arabidopsis*. *Plant Physiol.* 2012;**160**(1):396–406. <https://doi.org/10.1104/pp.112.201699>
- Wang W, Cai J, Wang P, Tian S, Qin G.** Post-transcriptional regulation of fruit ripening and disease resistance in tomato by the vacuolar protease SIVPE3. *Genome Biol.* 2017;**18**(1):47. <https://doi.org/10.1186/s13059-017-1178-2>
- Wang L, Feng Z, Wang X, Zhang X.** DEGseq: an R package for identifying differentially expressed genes from RNA-seq data. *Bioinformatics* 2010;**26**(1):136–138. <https://doi.org/10.1093/bioinformatics/btp612>
- Wang J, Liu X, Zhang A, Ren Y, Wu F, Wang G, Xu Y, Lei C, Zhu S, Pan T, et al.** A cyclic nucleotide-gated channel mediates cytoplasmic calcium elevation and disease resistance in rice. *Cell Res.* 2019;**29**(10): 820–831. <https://doi.org/10.1038/s41422-019-0219-7>
- Wang X, Prokhnevsky AI, Skarjinskaia M, Razzak MA, Streatfield SJ, Lee JY.** Facilitating viral vector movement enhances heterologous protein production in an established plant system. *Plant Biotechnol J.* 2023;**21**(3):635–645. <https://doi.org/10.1111/pbi.13977>
- Wang M, Rui L, Yan H, Shi H, Zhao W, Lin JE, Zhang K, Blakeslee JJ, Mackey D, Tang D, et al.** The major leaf ferredoxin Fd2 regulates plant innate immunity in *Arabidopsis*. *Mol Plant Pathol.* 2018;**19**(6):1377–1390. <https://doi.org/10.1111/mpp.12621>
- Wang K, Shao Z, Guo F, Wang K, Zhang Z.** The mitogen-activated protein kinase kinase TaMKK5 mediates immunity via the TaMKK5-TaMPK3-TaERF3 module. *Plant Physiol.* 2021;**187**(4): 2323–2337. <https://doi.org/10.1093/plphys/kiab227>
- Wang A, Shu X, Jing X, Jiao C, Chen L, Zhang J, Ma L, Jiang Y, Yamamoto N, Li S, et al.** Identification of rice (*Oryza sativa* L.) genes involved in sheath blight resistance via a genome-wide association study. *Plant Biotechnol J.* 2021;**19**(8):1553–1566. <https://doi.org/10.1111/pbi.13569>
- Wang X, Zhi P, Fan Q, Zhang M, Chang C.** Wheat CHD3 protein TaCHR729 regulates the cuticular wax biosynthesis required for

- stimulating germination of *Blumeria graminis* f.sp. *tritici*. *J Exp Bot*. 2019;**70**(2):701–713. <https://doi.org/10.1093/jxb/ery377>
- Wang Z, Zhou L, Lan Y, Li X, Wang J, Dong J, Guo W, Jing D, Liu Q, Zhang S, et al.** An aspartic protease 47 causes quantitative recessive resistance to rice black-streaked dwarf virus disease and southern rice black-streaked dwarf virus disease. *New Phytol*. 2022;**233**(6):2520–2533. <https://doi.org/10.1111/nph.17961>
- Wangdi T, Uppalapati SR, Nagaraj S, Ryu CM, Bender CL, Mysore KS.** A virus-induced gene silencing screen identifies a role for *Thylakoid Formation1* in *Pseudomonas syringae* pv *tomato* symptom development in tomato and *Arabidopsis*. *Plant Physiol*. 2010;**152**(1):281–292. <https://doi.org/10.1104/pp.109.148106>
- Want EJ, Wilson ID, Gika H, Theodoridis G, Plumb RS, Shockcor J, Holmes E, Nicholson JK.** Global metabolic profiling procedures for urine using UPLC-MS. *Nat Protoc*. 2010;**5**(6):1005–1018. <https://doi.org/10.1038/nprot.2010.50>
- Wei X, Shen F, Hong Y, Rong W, Du L, Liu X, Xu H, Ma L, Zhang Z.** The wheat calcium-dependent protein kinase TaCPK7-D positively regulates host resistance to sharp eyespot disease. *Mol Plant Pathol*. 2016;**17**(8):1252–1264. <https://doi.org/10.1111/mpp.12360>
- Weidenbach D, Jansen M, Franke RB, Hensel G, Weissgerber W, Ulferts S, Jansen I, Schreiber L, Korzun V, Pontzen R, et al.** Evolutionary conserved function of barley and *Arabidopsis* 3-KETOACYL-CoA SYNTHASES in providing wax signals for germination of powdery mildew fungi. *Plant Physiol*. 2014;**166**(3):1621–1633. <https://doi.org/10.1104/pp.114.246348>
- Wen Z, et al.** Integrating GWAS and gene expression data for functional characterization of resistance to white mould in soya bean. *Plant Biotechnol J*. 2018;**16**(11):1825–1835. <https://doi.org/10.1111/pbi.12918>
- Wibberg D, Andersson L, Tzelepis G, Rupp O, Blom J, Jelonek L, Pühler A, Fogelqvist J, Varrelmann M, Schlüter A, et al.** Genome analysis of the sugar beet pathogen *Rhizoctonia solani* AG2-2IIIB revealed high numbers in secreted proteins and cell wall degrading enzymes. *BMC Genomics* 2016;**17**(1):245. <https://doi.org/10.1186/s12864-016-2561-1>
- Wibberg D, Genzel F, Verwaaijen B, Blom J, Rupp O, Goesmann A, Zrenner R, Grosch R, Pühler A, Schlüter A.** Draft genome sequence of the potato pathogen *Rhizoctonia solani* AG3-PT isolate Ben3. *Arch Microbiol*. 2017;**199**(7):1065–1068. <https://doi.org/10.1007/s00203-017-1394-x>
- Wibberg D, Jelonek L, Rupp O, Hennig M, Eikmeyer F, Goesmann A, Hartmann A, Borriss R, Grosch R, Pühler A, et al.** Establishment and interpretation of the genome sequence of the phytopathogenic fungus *Rhizoctonia solani* AG1-IB isolate 7/3/14. *J Biotechnol*. 2013;**167**(2):142–155. <https://doi.org/10.1016/j.jbiotec.2012.12.010>
- Wibberg D, Rupp O, Jelonek L, Kröber M, Verwaaijen B, Blom J, Winkler A, Goesmann A, Grosch R, Pühler A, et al.** Improved genome sequence of the phytopathogenic fungus *Rhizoctonia solani* AG1-IB 7/3/14 as established by deep mate-pair sequencing on the MiSeq (Illumina) system. *J Biotechnol*. 2015;**203**:19–21. <https://doi.org/10.1016/j.jbiotec.2015.03.005>
- Winnenburg R, Baldwin TK, Urban M, Rawlings C, Köhler J, Hammond-Kosack KE.** PHI-base: a new database for pathogen host interactions. *Nucleic Acids Res*. 2006;**34**(Database issue):459–464. <https://doi.org/10.1093/nar/gkj047>
- Wu Y, Zhang L, Zhou J, Zhang X, Feng Z, Wei F, Zhao L, Zhang Y, Feng H, Zhu H.** Calcium-dependent protein kinase GhCDPK28 was identified and involved in *Verticillium* wilt resistance in cotton. *Front Plant Sci*. 2021;**12**:772649. <https://doi.org/10.3389/fpls.2021.772649>
- Xia Y, Fei B, He J, Zhou M, Zhang D, Pan L, Li S, Liang Y, Wang L, Zhu J, et al.** Transcriptome analysis reveals the host selection fitness mechanisms of the *Rhizoctonia solani* AG1IA pathogen. *Sci Rep*. 2017;**7**(1):10120. <https://doi.org/10.1038/s41598-017-10804-1>
- Xia Y, Suzuki H, Borevitz J, Blount J, Guo Z, Patel K, Dixon RA, Lamb C.** An extracellular aspartic protease functions in *Arabidopsis* disease resistance signaling. *EMBO J*. 2004;**23**(4):980–988. <https://doi.org/10.1038/sj.emboj.7600086>
- Yamamoto M, Nakatsuka S, Otani H, Kohmoto K, Nishimura S.** (+)-Catechin acts as an infection-inhibiting factor in strawberry leaf. *Phytopathology* 2000;**90**(6):595–600. <https://doi.org/10.1094/PHYTO.2000.90.6.595>
- Yang G, Li C.** General description of *Rhizoctonia* species complex. London: Plant pathology: INTECH Open; 2012.
- Yang CL, Liang S, Wang HY, Han LB, Wang FX, Cheng HQ, Wu XM, Qu ZL, Wu JH, Xia GX.** Cotton major latex protein 28 functions as a positive regulator of the ethylene responsive factor 6 in defense against *Verticillium dahliae*. *Mol Plant*. 2015;**8**(3):399–411. <https://doi.org/10.1016/j.molp.2014.11.023>
- Yang W, Xu X, Li Y, Wang Y, Li M, Wang Y, Ding X, Chu Z.** Rutin-mediated priming of plant resistance to three bacterial pathogens initiating the early SA signal pathway. *PLoS One* 2016;**11**(1):e0146910. <https://doi.org/10.1371/journal.pone.0146910>
- Yao L, Li Y, Ma C, Tong L, Du F, Xu M.** Combined genome-wide association study and transcriptome analysis reveal candidate genes for resistance to *Fusarium* ear rot in maize. *J Integr Plant Biol*. 2020;**62**(10):1535–1551. <https://doi.org/10.1111/jipb.12911>
- Ye J, Ding W, Chen Y, Zhu X, Sun J, Zheng W, Zhang B, Zhu S.** A nucleoside diphosphate kinase gene *OsNDPK4* is involved in root development and defense responses in rice (*Oryza sativa* L). *Planta* 2020;**251**(4):77. <https://doi.org/10.1007/s00425-020-03355-9>
- Yin W, Xiao Y, Niu M, Meng W, Li L, Zhang X, Liu D, Zhang G, Qian Y, Sun Z, et al.** ARGONAUTE2 enhances grain length and salt tolerance by activating *BIG GRAIN3* to modulate cytokinin distribution in rice. *Plant Cell* 2020;**32**(7):2292–2306. <https://doi.org/10.1105/tpc.19.00542>
- Yu HS, Ma LQ, Zhang JX, Shi GL, Hu YH, Wang YN.** Characterization of glycosyltransferases responsible for salidroside biosynthesis in *Rhodiola sachalinensis*. *Phytochemistry* 2011;**72**(9):862–870. <https://doi.org/10.1016/j.phytochem.2011.03.020>
- Yu Y, Ouyang Y, Yao W.** shinyCircos: an R/Shiny application for interactive creation of Circos plot. *Bioinformatics* 2018;**34**(7):1229–1231. <https://doi.org/10.1093/bioinformatics/btx763>
- Zhang C, Gao H, Li R, Han D, Wang L, Wu J, Xu P, Zhang S.** GmBTB/POZ, a novel BTB/POZ domain-containing nuclear protein, positively regulates the response of soybean to *Phytophthora sojae* infection. *Mol Plant Pathol*. 2019;**20**(1):78–91. <https://doi.org/10.1111/mpp.12741>
- Zhang K, He M, Fan Y, Zhao H, Gao B, Yang K, Li F, Tang Y, Gao Q, Lin T, et al.** Resequencing of global Tartary buckwheat accessions reveals multiple domestication events and key loci associated with agronomic traits. *Genome Biol*. 2021;**22**(1):23. <https://doi.org/10.1186/s13059-020-02217-7>
- Zhang L, Li X, Ma B, Gao Q, Du H, Han Y, Li Y, Cao Y, Qi M, Zhu Y, et al.** The Tartary buckwheat genome provides insights into rutin biosynthesis and abiotic stress tolerance. *Mol Plant*. 2017;**10**(9):1224–1237. <https://doi.org/10.1016/j.molp.2017.08.013>
- Zhang K, Logacheva MD, Meng Y, Hu J, Wan D, Li L, Dagmar J, Wang Z, Georgiev MI, Yu Z, et al.** Jasmonate-responsive MYB factors spatially repress rutin biosynthesis in *Fagopyrum tataricum*. *J Exp Bot*. 2018;**69**(8):1955–1966. <https://doi.org/10.1093/jxb/ery032>
- Zhang H, Yohe T, Huang L, Entwistle S, Wu P, Yang Z, Busk PK, Xu Y, Yin Y.** dbCAN2: a meta server for automated carbohydrate-active enzyme annotation. *Nucleic Acids Res*. 2018;**46**(W1):W95–W101. <https://doi.org/10.1093/nar/gky418>
- Zhang YL, Zhang CL, Wang GL, Wang YX, Qi CH, Zhao Q, You CX, Li YY, Hao YJ.** The R2R3 MYB transcription factor MdMYB30 modulates plant resistance against pathogens by regulating cuticular wax biosynthesis. *BMC Plant Biol*. 2019;**19**(1):362. <https://doi.org/10.1186/s12870-019-1918-4>
- Zhao H, He Y, Zhang K, Li S, Chen Y, He M, He F, Gao B, Yang D, Fan Y, et al.** Rewiring of the seed metabolome during Tartary buckwheat domestication. *Plant Biotechnol J*. 2023;**21**(1):150–164. <https://doi.org/10.1111/pbi.13932>

- Zhao J, Li L, Liu Q, Liu P, Li S, Yang D, Chen Y, Pagnotta S, Favery B, Abad P, et al.** A MIF-like effector suppresses plant immunity and facilitates nematode parasitism by interacting with plant annexins. *J Exp Bot.* 2019;**70**(20):5943–5958. <https://doi.org/10.1093/jxb/erz348>
- Zhao BR, Zheng Y, Gao J, Wang XW.** Maturation of an antimicrobial peptide inhibits *Aeromonas hydrophila* infection in crayfish. *J Immunol.* 2020;**204**(3):487–497. <https://doi.org/10.4049/jimmunol.1900688>
- Zheng A, Lin R, Zhang D, Qin P, Xu L, Ai P, Ding L, Wang Y, Chen Y, Liu Y, et al.** The evolution and pathogenic mechanisms of the rice sheath blight pathogen. *Nat Commun.* 2013;**4**:1424. <https://doi.org/10.1038/ncomms2427>
- Zhou M, Memelink J.** Jasmonate-responsive transcription factors regulating plant secondary metabolism. *Biotechnol Adv.* 2016;**34**(4):441–449. <https://doi.org/10.1016/j.biotechadv.2016.02.004>
- Zhou M, Sun Z, Ding M, Logacheva MD, Kreft I, Wang D, Yan M, Shao J, Tang Y, Wu Y, et al.** FtSAD2 and FtJAZ1 regulate activity of the FtMYB11 transcription repressor of the phenylpropanoid pathway in *Fagopyrum tataricum*. *New Phytol.* 2017;**216**(3):814–828. <https://doi.org/10.1111/nph.14692>
- Zhu Z, Zhang F, Hu H, Bakshi A, Robinson MR, Powell JE, Montgomery GW, Goddard ME, Wray NR, Visscher PM, et al.** Integration of summary data from GWAS and eQTL studies predicts complex trait gene targets. *Nat Genet.* 2016;**48**(5):481–487. <https://doi.org/10.1038/ng.3538>
- Zrenner R, Verwaaijen B, Genzel F, Flemer B, Grosch R.** Transcriptional changes in potato sprouts upon interaction with *Rhizoctonia solani* indicate pathogen-induced interference in the defence pathways of potato. *Int J Mol Sci.* 2021;**22**(6):3094. <https://doi.org/10.3390/ijms22063094>